IEEE Journal of Microwaves

MTT-S MHz to THz Community

Received 5 January 2023; revised 28 February 2023 and 17 May 2023; accepted 31 May 2023. Date of current version 7 July 2023.

Digital Object Identifier 10.1109/JMW.2023.3282875

Terahertz Sources and Receivers: From the Past to the Future

SUMER MAKHLOUF [1], OLEG COJOCARI [2], MARTIN HOFMANN [3], TADAO NAGATSUMA [4] (Fellow, IEEE), SASCHA PREU [5] (Member, IEEE), NILS WEIMANN [6] (Member, IEEE), HEINZ-WILHELM HÜBERS [7], AND ANDREAS STÖHR [8] (Senior Member, IEEE)

(Invited Paper)

[1]Microwave Photonics GmbH, 57047 Oberhausen, Germany
[2]ACST GmbH, 63457 Hanau, Germany
[3]Photonics and Terahertz Technologies, Ruhr Universität Bochum, 44801 Bochum, Germany
[4]Graduate School of Engineering Science, Osaka University, Osaka 560–0853, Japan
[5]THz Devices and Systems, Technische Universität Darmstadt, 64283 Darmstadt, Germany
[6]Components for High Frequency Electronics, University of Duisburg-Essen, 47057 Duisburg, Germany
[7]German Aerospace Center (DLR), 12489 Berlin, Germany
[8]Optoelectronics, University of Duisburg-Essen, 47057 Duisburg, Germany

CORRESPONDING AUTHOR: Sumer Makhlouf (e-mail: sumer.makhlouf@microwave-photonics.com).

This work was supported by the Deutsche Forschungsgemeinschaft (DFG), German Research Foundation under Grant 287022738-TRR 196.

ABSTRACT The rapid progress in semiconductor technology has vastly boosted the development of terahertz sources and receivers in terms of compactness, reliability, operation frequency, and output power. In this manuscript, we report on the latest achievements in terahertz sources and receivers and provide a comprehensive overview of their working principles and applications in THz systems.

INDEX TERMS THz technologies, THz photodiodes, THz photoconductors, THz semiconductor laser diodes, THz quantum cascade lasers, THz heterojunction bipolar transistors, THz high electron mobility transistor, THz resonant tunneling diodes, THz Schottky barrier detectors and mixers.

I. INTRODUCTION

A number of breakthroughs in photonics and electronics made since the early 1990s have helped to mature terahertz (THz) technologies and transfer THz applications from the laboratory stage to commercial applications. Meanwhile, the technology readiness level of THz systems in communications, imaging, and spectroscopy has reached the level of real-world use. Further applications, foremost in biomedical sensing and agriculture, are getting increased attention. In this review, we will address the state-of-the-art in semiconductor-based photonic and electronic THz sources and receivers operating in the frequency range between 100 GHz and 10 THz.

Terahertz has long been an unexplored range of the electromagnetic spectrum, mainly because of the difficulties in realizing powerful sources and efficient receivers. The German scientist Heinrich Rubens was the first to study the frequency gap in the electromagnetic spectrum between infrared and electronic sources [1]. In 1897, H. Rubens and E.F. Nichols first formulated the intention to extend knowledge and bridge the gap between electronics and photonics [2].

Later on, this was often referred to as the "THz gap" in scientific works. Since then, numerous achievements have been made to bridge the THz gap, especially in developing sources and receivers [2], [3], [4]. This article explores recent progress in semiconductor-based photonic and electronic THz sources and receivers. The focus is on those sources and receivers that can be operated at ambient temperature or with moderate cooling. Devices that require extensive cooling, such as superconductor-insulator-superconductor (SIS) mixers, are not considered in this review article. However, the reader should be aware that THz receivers based on cooled superconductors are widespread in astronomy, and major discoveries have been made with superconducting THz receivers implemented in ground-based observatories such as ALMA (Atacama Large Millimeter Array) [5] or in airborne and satellite observatories such as SOFIA (Stratospheric Observatory for Infrared Astronomy) [6] and Herschel Space Observatory

This work is licensed under a Creative Commons Attribution 4.0 License. For more information, see https://creativecommons.org/licenses/by/4.0/

[7]. One example is recent images of a black hole's shadow obtained using global very long baseline interferometry and THz heterodyne receivers operating at about 228 GHz [8].

With respect to photonic THz sources in Section II, the manuscript reports the state-of-the-art of optical down-conversion sources, quantum cascade lasers (QCLs), uni-travelling carrier photodiodes (UTC-PDs), and photoconductors. As for photonic THz receivers in Section III, the paper covers photoconductors. Section IV focuses on electronic chip-level sources, including state-of-the-art CMOS-based sources, heterojunction bipolar transistors (HBTs), high electron mobility transistors (HEMTs), and resonant tunneling diodes (RTDs). Also, Schottky barrier diode (SBD) multipliers for THz generation are addressed. Finally, in Section V, direct electronic THz detectors, like SBDs and field effect transistors (FETs), as well as electronically and optically pumped heterodyne receivers, are discussed.

II. PHOTONIC TERAHERTZ SOURCES

Based on the employed photonic source, photonic THz systems can be categorized into time domain or frequency domain. Time domain systems mainly utilize optical down-conversion by heterodyning two pulsed laser beams in high-speed convertors, such as photoconductive antennas, to down-convert the light into THz signals. On the other hand, frequency domain systems employ continuous wave (CW) laser beams that can be either similarly down-converted into THz signals or directly emitted in the THz domain by using, for example, quantum cascade lasers (QCLs).

A. OPTICAL DOWN-CONVERSION

During the past three decades, various impressive applications for photonic-assisted THz systems have been presented [9]. These applications include, for example, various spectroscopic systems for liquid [10], solid [11], and gaseous [12] samples, THz communication [13], and non-destructive testing in industrial settings [14]. Despite numerous laboratory studies that have impressively demonstrated the application potential of photonic-assisted THz systems, the majority of them are still expensive and complex, preventing their use in industry [14]. A major step toward reducing both cost and complexity is taken by replacing complex photonic sources, like Ti:Sapphire or fiber lasers, with diode lasers [10]. Diode lasers have a footprint below 1 mm^3 and, additionally, enable monolithic integration into compact THz systems. A major application field of photonic-assisted THz systems that exploit diode lasers is spectroscopic systems that can be further differentiated into frequency domain systems (FDS) [15], [16], time domain spectroscopy (TDS) systems [17], [18], [19], and quasi-TDS (QTDS) systems [20], [21], [22]. In all systems, the use of telecom components at a 1.55 μm wavelength is an important enabler for developing compact, cost-effective, and robust systems for industrial applications [23], [24].

Photonic spectroscopy systems follow a general homodyne concept, as schematically shown in Fig. 2. The output of the near-infrared (NIR) photonic source is split into two parts with a beam splitter. One part propagates to the THz transmitter, which may be a uni-travelling carrier photodiode (UTC-PD) (section C) or a photoconductor (section D). The THz signal propagates through the THz path, which may include samples under test, and then reaches the THz receiver, which is often realized using a photoconductor (Section III-A). The photonductor is pumped with an optical reference signal that is provided by the second part of the source beam that has passed through a variable delay line for sampling. Depending on the concept, the NIR diode laser source can be either a two-color CW signal (FDS), a short pulse source (TDS), or a broadband CW source (QTDS).

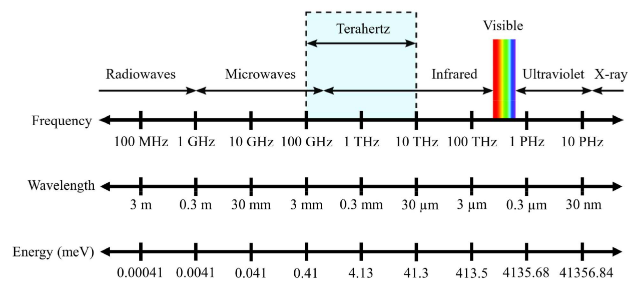

FIGURE 1. Electromagnetic spectrum between millimeter-wave and UV. Today, Terahertz waves are commonly referred to as frequencies ranging between 100 GHz and 10 THz, i.e., wavelengths between several 10s of μm up to 3 mm. This corresponds to energy levels between ~0.4 meV up to several 10's meV.

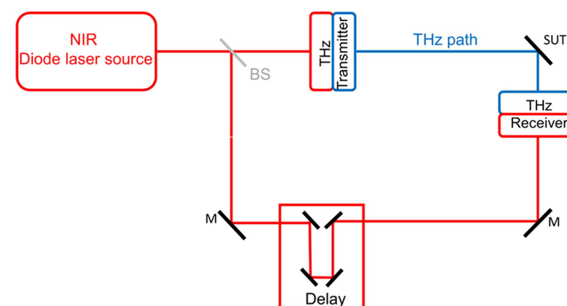

FIGURE 2. Homodyne concept for diode-laser based photonic THz systems. BS: beam splitter, SUT: sample under test, M: mirror.

1) FREQUENCY DOMAIN SYSTEMS

In photonic THz FDS systems, the NIR diode laser source comprises two single-frequency signals, the difference frequency of which is generated via photomixing [25]. Photomixing can be performed with transmitters like nonlinear crystals, photoconductive antennas [25], or photodiodes [26]. The generated THz signal interacts with the sample under test and is then detected by a receiver. This can either be a thermic THz detector like a bolometer [27] for incoherent detection or, more conveniently in modern systems, a heterodyne mixer [5] or a photoconductive antenna for coherent detection [28]. In such a coherent homodyne THz system as shown in Fig. 2, sampling of the received THz signal is required and is sometimes performed by introducing a mechanical delay line into the system. Other systems retrieve the amplitude and

phase information from a frequency sweep, for example, with the aid of a Hilbert transformation. The two single-frequency near-infrared laser signals can fundamentally be generated in different ways.

Commercial FDS systems often contain two stabilized, separate distributed feedback (DFB) lasers. However, the stabilization of the lasers and the beam combination on the transmitter introduce complexity. Thus, two-color lasers, i.e., laser systems thatf emit simultaneously on two wavelengths with a well-defined difference frequency, were suggested and implemented into THz FDS systems [29], [30], [31]. While external cavity diode lasers with spectral filtering in the resonator provide enormous flexibility in terms of the tunability of the generated THz frequency, monolithic two-color diode lasers are more attractive for integration into compact THz systems. Such monolithic two-color diode lasers have been demonstrated on the basis of distributed Bragg reflector (DBR) [32] and DFB lasers [29]. While both have been successfully implemented into THz FDS systems, the performance of the THz FDS system crucially depends on the performance of the two-color lasers. Most importantly, stable two-color operation on two single modes is required. Moreover, for spectroscopic and metrological applications, continuous tuning of the difference frequency is desirable. While Y-shaped two-color DBR lasers have been shown to suffer from mode hops [32] that induce severe problems for measurements requiring frequency tuning, Y-shaped slotted DFB lasers have been demonstrated with continuous mode hop-free tuning across 10.5 GHz at 1 THz center frequency [33]. Such lasers enable precise thickness measurements in non-destructive testing. For example, the thickness and refractive index of different silicon wafers could be determined with sufficient accuracy (better than 10%) with such a system [34]. Moreover, the continuous frequency tuning enables the mechanical delay line in the homodyne system to be waived. Thus, such lasers are perfect candidates for integrated THz FDS systems.

2) TIME DOMAIN SPECTROSCOPY SYSTEMS

The outstanding performance of THz TDS systems opens up the way to apply THz technology in a wide range of applications, ranging from material characterization to chemistry and biology applications [35], [36]. THz TDS provides information about the spectral fingerprints of numerous substances, enabling the identification of substances such as pharmaceuticals and explosives. Other applications are in the area of non-destructive testing, for example, the measurement of paint thicknesses in the automotive industry. In a THz TDS system, the NIR source is a femtosecond laser [10], [35]. Femtosecond laser pulses generate a broadband THz transient in the THz transmitter, which propagates through the THz path, interacts with the sample under test, and is then sampled at the receiver (either by using a photoconductive antenna or by electro-optic sampling) by mixing the incoming modified THz transient with a second delayed portion of the femtosecond pulse. Varying the delay of this second pulse, for example, via a mechanical delay stage, provides the THz signal, and the Fourier transformation delivers its THz spectrum [36]. This way, broadband THz spectra with bandwidths up to several THz can be obtained. The THz bandwidth not only depends on the THz transmitter and receiver but also on the width of the femtosecond pulses. Standard sources for THz TDS systems are femtosecond Ti:Sapphire and fiber lasers. However, these lasers are still rather complex and expensive, and consequently, complexity and high cost transfer to THz TDS systems based on such lasers.

For compact TDS systems, it is thus desirable to consider chip-sized short-pulse lasers like diode lasers. However, diode lasers usually provide only moderate power in the few mW range with pulse widths of a few picoseconds, while TDS systems require several tens of mW of output power and pulse widths in the sub-picosecond range. Recently, diode lasers yielding sufficient output power were developed. These lasers contain a passively mode-locked external cavity laser diode with a subsequent tapered laser diode amplifier to reach the required power level of about 500 mW average power [37]. Moreover, the pulses emitted from diode lasers are usually strongly chirped. Therefore, the system also contained a compressor to achieve pulse widths in the range of 300 fs [38]. This shoebox-sized femtosecond laser system was successfully implemented into a standard THz TDS system and provided a THz bandwidth of about 0.6 THz [18].

However, reducing the complexity of such a TDS system and limiting its footprint with the vision of a fully integrated TDS on a chip system still faces several challenges. A standard TDS system includes a mechanical delay line, introducing complexity as well as reducing the sampling speed. Both may be overcome by implementing alternative sampling concepts, for example, asynchronous optical sampling (ASOPS) [39], [40], [41], [42]. The idea of ASOPS is to operate two separate mode-locked laser diodes (MLLDs) for gating transmitter and receiver. The two lasers are similar but operate at slightly different repetition frequencies. Thus, at the receiver, the THz signal is sampled at the difference frequency of the repetition frequencies of the two lasers. This concept was implemented successfully with two MLLD systems [43]. However, the system only provided 0.5 THz of bandwidth and requires further optimization, and, most importantly, it is still rather complex. This can be overcome by replacing the external cavity laser diodes with monolithically mode-locked devices, as suggested in [41]. The current generation of monolithically MLLDs provides sufficient output power in the order of several tens to hundreds of mW at pulse widths in the low picosecond to sub-picosecond range. Such devices, together with the ASPOS technique, may lay the basis for fully integrated THz TDS systems. However, it has to be considered that these monolithic MLLDs have high repetition rates in the range of up to 50 GHz [19]. These ultra-high repetition rate (UHRR) THz TDS systems, accordingly, have a lower frequency resolution compared to THz FDS systems [44]. Moreover, the emitted pulses are often chirped, and pulse

widths are not shorter than a few picoseconds without chirp compensation.

3) QUASI-TDS SYSTEMS

A further possibility to reduce the complexity of THz spectroscopy systems is to implement quasi-time domain spectroscopy (QTDS) [22]. This concept combines the ideas of photomixing and TDS. Instead of using MLLDs, broadband light sources like, in the simplest case, multi-mode NIR laser diodes are used as optical sources, as shown in Fig. 2. Generally, the wideband optical spectrum of a MLLD contains multiple modes with a constant difference frequency. This allows the generation of multiple THz frequencies by exploiting different pairs of modes that are superimposed in the THz path and can be detected as a QTDS transient at the receiver.

Though commercial multi-mode laser diodes are extremely compact and easy to operate in a QTDS system, the generated THz spectrum cannot be further optimized. In contrast, external cavity arrangements with spectral filtering enable control of the THz spectrum [21]. It was shown that in an external cavity configuration named the Fourier transform external cavity, the diode laser spectrum could be tailored by spectral filtering [21]. Broadband emission with variable bandwidth could be obtained, as could two-color operation for photomixing [21]. Though extremely flexible, such external cavity arrangements are complex and not suitable for future integration. Another option for QTDS that may enable integration and sufficient bandwidth is to operate the monolithically mode-locked high repetition rate diode lasers in a QTDS system that only requires large bandwidth but not extremely short optical pulse widths.

B. QUANTUM CASCADE LASERS

In contrast to optical down-conversion sources, quantum cascade lasers (QCLs) are direct optical THz emitters. Photons in QCLs are generated by electron transitions between two energy states in the conductance band (intraband transitions) [45]. These states are formed by coupled multiquantum wells and barriers, as shown in Fig. 3 [46]. Because the transition energy between two states in a QCL is low compared to interband transitions in conventional laser diodes, photon emissions typically occur in the mid-infrared to far-infrared (THz) spectral range. The major drawback of THz QCLs is that carrier inversion is hindered by the onset of thermally activated nonradiative scattering processes, which require the laser to be operated at low temperatures. The first THz QCL was demonstrated in 2002 [47]. Meanwhile, QCLs have been demonstrated for THz frequencies in the range between ~1.3 THz and ~5.4 THz [48]. Also, the operating temperatures for QCLs were continuously increased [47].

Recently, these efforts led to a pulse-mode 4 THz QCL lasing at 250 K [49]. So far, despite the impressive progress, the cooling requirement for THz QCLs has somewhat limited their usage to rather specialized applications such as local oscillators in the GREAT (German Receiver for Astronomy at THz frequencies) heterodyne spectrometer on board of SOFIA or in a stratospheric balloon [50], [51], [52]. Here, a QCL used as LO should have a decent operating temperature (typically at least about 50 K in order to be operated in a compact cryocooler) but at the same time provide sufficient output power (typically in the mW range) in CW mode and in the fundamental Gaussian-shaped beam with high frequency stability and high frequency tunability [53].

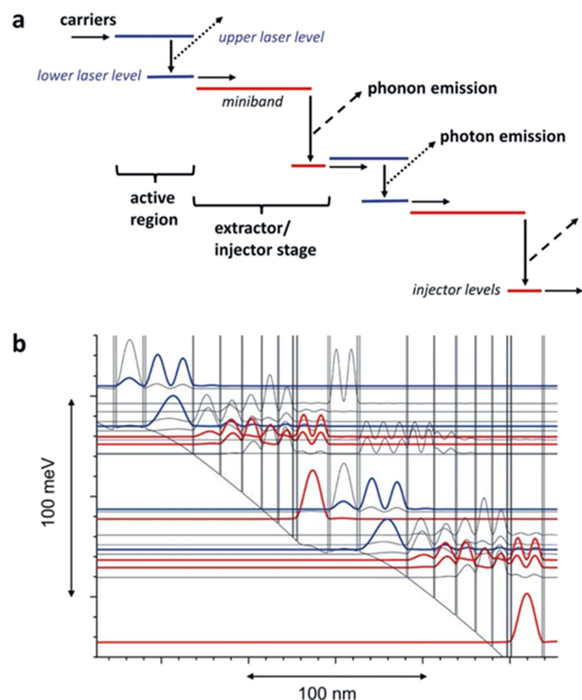

FIGURE 3. (a) Schematic concept of a QCL showing the cascaded stages in the active region and the intra band transitions of electrons between the upper and lower laser levels (b) Detailed subband structure of a QCL operating at 4.7 THz. The laser states are in blue. From [46], © [2020] Photoniques.

An interesting new approach that has been pioneered in [54] allows room-temperature THz generation using QCLs, as demonstrated in [55], [56], [57]. In this approach, THz difference frequency generation in the range from about 1 THz to 6 THz can be achieved in mid-IR QCLs operating at room temperature.

C. UNI-TRAVELLING CARRIER PHOTODIODES

In 1997, Ishibashi et al. demonstrated a new type of photodiodes called uni-travelling-carrier photodiodes (UTC-PDs), which could operate faster with wider output linearity or higher saturation current than conventional PIN photodiodes [58]. The featured structure of the original UTC-PD has a relatively thin p-type absorption layer, where electrons are generated as minority carriers, diffused, and/or accelerated toward the collection layer. In the depleted collection layer, electrons travel at a ballistically high velocity. Thus, the contribution of slow hole transport to the response of the PD can be effectively excluded in the UTC-PD.

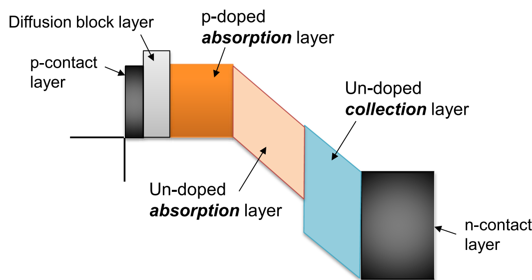

FIGURE 4. Band diagram of a UTC-PD with modified absorber to optimize the efficiency and speed. There are various types of absorber layer designs.

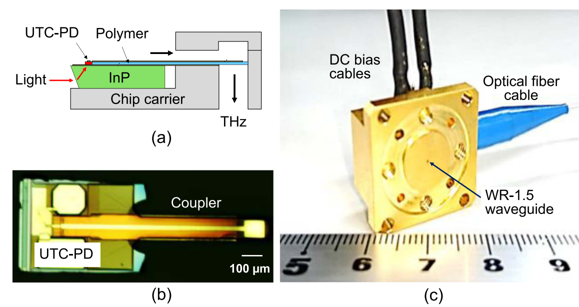

FIGURE 5. 600 GHz UTC-PD module with WR-output (a) Simplified structure of the module (b) Photograph of the coupler-integrated UTC-PD chip (c) Photograph of the UTC-PD module.

Since the invention of the UTC-PDs, various modifications have been proposed for layer structures to improve their performance. To decrease the electron traveling time in the absorption layer, the introduction of a quasi-field into the absorption layer by means of band-gap grading and/or doping grading is effective. Moreover, to decrease the saturation in electron velocity in the collection layer, n-type doping or cliff-like structures are effective for the optimization of the electric field profile, while moderate n-type doping in the collection layer is preferable to increase the saturation current. A combination of neutral and depleted absorption layers increases the responsivity without considerably sacrificing the saturation current or operation speed. The use of a dual-depletion region is also effective in this modification to maintain high-speed operation. Another way to improve the responsivity while maintaining the operation speed is to employ an external structure to guide the input light to the absorption layer at different angles, such as a waveguide structure, evanescent coupling, velocity-matched distributed, refracting facet, or total reflection structure. The optical resonant cavity structure is also effective in providing enhanced sensitivity.

Fig. 4 shows a typical layer structure of the modified UTC-PD, which optimizes a trade-off between the bandwidth and the responsivity, where UTC and PIN structures are compositely employed. This structure can still be modified, for example, graded doping can be applied to a p-type absorber to yield an effective quasi-field to speed up electrons. For more details, we direct the interested reader to the references [59], [60].

For practical applications, UTC-PDs are usually integrated either with planar antennas such as bow-tie, patch, or slot antennas or with transitions from coplanar waveguides (CPWs) to rectangular waveguides (WRs). In the former integration approach, a semi-spherical silicon lens is usually attached to the backside of the substrate to collimate the radiated beam, resulting in an increase in total antenna gain as large as 40 dBi at 300 GHz [61]. For UTC-PD packages with WR-outputs, transitions are employed to efficiently couple RF signals generated by the UTC-PDs to the WRs. Here, the transitions can be integrated with the UTC-PDs in either a hybrid or monolithic approach. Hybrid integration of a quartz-based transition with a UTC-PD has been successfully demonstrated for commercial modules up to about 400 GHz [62]. On the other hand, monolithic integration of a UTC-PD with a transition that is based either on a thinned indium phosphide (InP) substrate [63] or on a membrane thin-film using polymeric dielectric material [64] has been presented, as shown in Fig. 5. It is noteworthy to indicate that the transition presented in [63] is scalable up to 2.2 THz.

The maximum reported output power from UTC-PD chips or modules is over 10 mW at 100 GHz, about 1 mW at 300 GHz, and about 10 μW at 1 THz [65], [66]. Pulse-like excitation is demonstrated to be effective in enhancing the output power by a factor of two to three compared to CW excitation [67]. Furthermore, using monolithically integrated impedance matching circuits with UTC-PDs has been shown to increase the output power by a factor of two or three by reducing the RC-limit [68].

For real-world THz applications, such as THz communications, more output power is needed. One of the major limitations of the RF output power from photodiodes is their heat dissipation capability. Thus, external heat sink structures or heterogeneous substrates featuring higher thermal conductivity, such as silicon carbide (SiC) or diamond, are necessary. This allows not only higher output power but also more reliability by increasing the diode chip lifetime [69]. Moreover, a substantial enhancement of the output power can be achieved by power combining. There are mainly three approaches to power combining. The first approach is based on using electrical power combiner circuits, where low-loss transmission lines like dielectric waveguides can be employed as transitions between the UTC-PDs and the power combiner [70]. The second approach is based on spatial power combination by using an array of antennas, such as the demonstrated array of patch antenna-integrated RTDs [71] and array of antenna-integrated UTC-PDs for beam steering [72]. These power-combining techniques should be improved to the level of electronics-based phased array transmitters and receivers. The third approach is based on using multilayer packaging technology to integrate an array of UTC-PDs with a WR-power combiner [73].

D. PHOTOCONDUCTORS

The classic version of a photoconductive source consists of a highly resistive semiconductor that is switched to a low

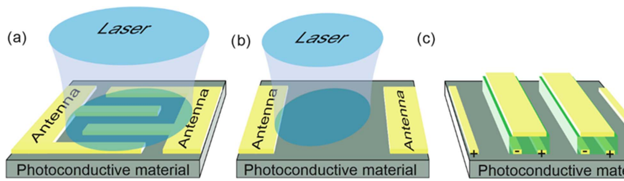

FIGURE 6. General setups of photoconductors: (a) Planar finger electrodes for continuous-wave (CW) operation (b) fingerless gap attached to an antenna for pulsed operation. Frequently, the laser spot is misplaced closer to the positive electrode where electrons are collected (c) antenna-less large area emitters. Every second gap is blocked (indicated by a green dielectric covered with a metal) or etched away in order to prevent destructive interference in the far field. The laser (omitted) illuminates a large area. While in (a) and (b) antennas are frequently used, in (c) the separated charges directly radiate the THz radiation.

resistance by an incident optical signal, as illustrated in Fig. 6 for the three most prominent cases. The switching takes place via absorption and is therefore a linear effect. An applied DC bias separates electrons from holes in order to generate a current. If the optical signal contains an AC envelope component, the photoconductor will generate an AC current that is proportional to the AC optical component as well as a DC current that is proportional to the average optical power [25].

In most cases, an on-chip antenna (Fig. 6(a) and (b)) converts the AC current component into a free-space AC (i.e., THz) signal. In large-area emitter concepts, the radiation originates directly from electrons or holes drifting to the respective contacts (Fig. 6(c)). The optical AC component may result from mixing two (or more) CW laser signals, a broadband laser pulse, or further variants discussed in Section II-A.

The photoconductive material must be optimized for the respective operation conditions. This leads to the following requirements: 1. high absorption at the driving laser frequency, 2. a high charge mobility (typically $>$ a few 100 cm^2/Vs) for large currents at a given bias field, 3. a high break-down field strength for photoconductive sources, 4. a high resistance, and 5. for CW and detectors, a short carrier life time (typically $<$ 0.5 ps).

Unfortunately, these requirements are partially conflicting. For brevity, we direct the interested reader to the references [25], [74], [75], [76], where the details on carrier transport and derivations of the photocurrent and roll-offs are elaborated. In the following, we will provide a brief review of the realizations of photoconductors and new technologies, partly overcoming requirements 1–5.

Historically, the first photoconductors consisted of semi-insulating or low-temperature-grown GaAs (LT-GaAs), InP, and radiation-damaged silicon in the mid- to late 1980s. They were only used under pulsed operation without any antenna. The AC current directly radiates the THz field, similar to the case illustrated in Fig. 6(c), but with only one, very wide electrode gap of several millimeters. A high bias (several kV) was needed in order to achieve a noteworthy DC field for separating optically generated charges. Between the electrodes, the large semiconductor aperture was hit with a very powerful laser (typically several μJ). They were consequently named “large aperture emitters” or, after their inventor, “Auston switch” [77], already reaching THz peak powers in the few watt level at a repetition rate of 8.3 kHz. The modern version of the large aperture emitter is the large area emitter, where a large semiconductor area is covered with electrodes spaced by a few 10 μm as shown in Fig. 6(c). This allows to considerably reduce the bias voltage and still attain high THz powers. Every second gap is etched away or blocked in order to yield constructive interference in the far field. Dekorsy et al. have demonstrated average powers of 1.5 mW at a near-infrared to THz conversion efficiency of 0.2% [78].

Many groups focus on lumped-element, antenna-coupled devices that can be operated with considerably lower laser power of the order of a few 10 mW using table-top laser systems. In the mid-1990s, LT-GaAs was optimized and combined with logarithmic-periodic or logarithmic spiral antennas, reaching a maximum frequency of 3.8 THz and somewhat less than 1 μW at 1 THz [15]. With the advent of telecom lasers and erbium amplifiers, materials suitable for operation at 1550 nm were researched. LT-GaAs and ErAs:GaAs show absorption via mid-gap trap states [79], with promising results at 1550 nm operation, though direct inter-valley absorption is more efficient. The first low-lifetime semiconductors, based on low-temperature-grown InGaAs, have unfortunately shown severe background conductance. [80]. This problem remained as the ion damage also caused states close to the conduction band edge. It took till the late 2000s before p-type doped LT-InGaAs in combination with InAlAs layers resulted in efficient, competitive THz sources [81]. To further improve the material, new additives to InGaAs were investigated in order to yield mid-gap trap states. These include, in particular, iron and rhodium, leading to the so far highest reported average power of a lumped-element photoconductive source under pulsed operation of 0.637 mW and a bandwidth of 6.5 THz with only 28 mW of laser power [82]. In parallel, the development of ErAs:InGaAs:InAlAs superlattices evolved. They have achieve to date an output power under pulsed operation of 0.472 mW and a bandwidth of 6.5 THz at a laser power of 42 mW [83].

Besides these rather classical approaches of engineering the trap states in InGaAs or GaAs, several new approaches emerged, partially circumventing requirements 1–5. Plasmonic-enhanced electrodes consist of a narrow grating instead of a fully metallized contact. The grating is optimized to strongly increase the absorption close to the grating electrodes by exciting plasma waves in the metal. This strongly confines the absorption of light very close to the positive electrode, where the faster electrons are collected very efficiently as they only need to travel ~100 nm [84]. This results in high gain even if the material has a low carrier lifetime. For CW operation, the requirement 4 and thermal management can be mitigated by using low duty cycles. In [76], the authors achieved 0.8 mW peak THz power (16 μW average power) at 2% duty cycle at 150 mW laser power in combination with plasmonic electrodes on ErAs:InGaAs.

A pathway to circumvent the requirement 3 and also reduce the thermal load aims for bias-free operation. The Photo-Dember effect has been instrumentalized in large-area emitters [85]. A more recent approach uses devices with a pronounced surface field by grading the semiconductor [86]. While the Dember effect is caused by diffusion, the surface field drifts carriers, which enhances the device's efficiency. The authors report an average THz power of 0.86 mW at 0.9 W optical power at 1550 nm in a large area emitter configuration.

Finally, a completely different approach discards semiconductors and uses the inverse spin-hall effect in a stack of metals. By implementing a sequence of very thin, partially optically transparent magnetized ferromagnetic and non-magnetic films, absorbed light creates a spin-imbalance. The spin current that drifts away from the generation point is transformed into a charge current at the interface between the ferromagnetic and the non-magnetic film [87]. The beauty of this approach is that it is compatible with most laser wavelengths, there is no lifetime roll-off, and it is possible to deposit the inexpensive layer sequence on any host material. Emitted spectra extending beyond 30 THz have been demonstrated using an unstructured large-area film. Also, antenna-coupled lumped-element spintronic emitters were demonstrated recently under pulsed operation [88].

III. PHOTONIC TERAHERTZ RECEIVERS

A. PHOTOCONDUCTORS

Similar to photoconductive sources (Section II-D), photoconductive receivers absorb a laser signal that contains at least two (CW, quasi-CW) or many (TDS, QTDS) frequencies with a frequency difference in the THz range. The absorbed laser signal, *P_L (t)*, modulates the conductivity of the photoconductor at these difference frequencies, $\sigma(t, \Delta f_L) \sim P_L(t)$, where Δf_L is a (potentially continuous) variable containing all possible difference frequencies of the laser signal as well as a DC term, with an amplitude proportional to the total incident laser power. As opposed to sources, there is no DC-bias applied. Instead, the bias originates from an incident THz wave that is, in most cases, transformed to a THz bias, $U_{THz}(\mathrm{t}) \sim \mathrm{E_{THz}(t)}$, by an antenna. The bias separates electrons and holes generated by the optical signal, i.e., the photoconductor acts as a mixer of the optical envelope and THz signal.

We remark that $\sigma(t, \Delta f_L)$ is fairly complicated to calculate as optically generated carriers remain in the semiconductor for a certain time and therefore increase the conductance for an extended period of time after their generation [89]. In the case of a homodyne CW spectrometer, a UTC diode or a photoconductive source is operated with the identical pair of lasers as the receiver, i.e., $|\Delta \mathrm{f_L} - \mathrm{f_{THz}}| = 0$, mixing of the optical envelope and the THz wave yields a DC current $\mathrm{I} \sim \mathrm{E_{THz} P_L} \cos\varphi$, where φ originates from a path length difference between source and receiver path [90], as well as THz frequency components that cannot be detected by post-detection electronics. If the laser signal is a broadband pulse, the mixing is easier to evaluate in the time domain. The Fourier transform of the phase of the signal turns into a time delay, τ, which is frequently swept by a delay line. Sweeping over all possible delays τ results in the correlation measurement of $\sigma(t)$ and $E_{THz}(t)$. This is the basic concept of THz-TDS, where a photoconductive source is driven by the same laser pulse as the photoconductive receiver. Likewise, this case covers QTDS and cross-correlation spectroscopy (CCS). We remark that the relative delay, τ, is only well defined if the laser signal driving the source is the same (or phase-locked, as in the case of asynchronous optical sampling, ASOPS) to the signal arriving at the receiver. The detection principle also works for cases where $|\Delta f_L - f_{THz}| \neq 0$, i.e., heterodyne detection or signals with an arbitrary, broadband spectrum, where laser signal and THz signal are not necessarily phase-locked. This was applied, for example, in photonic spectrum analyzers, where the optical signal consisted of a single, spectrally pure beat note (i.e., two lasers detuned by the desired THz frequency $\Delta \mathrm{f_L}$) and the THz field originated from a source under test with an unknown spectrum [91], [92]. As the relative phase between the two is not locked and thus randomly changing, only the power spectral density of the down-converted current is recorded and phase information is discarded.

The materials used for photoconductive receivers are typically very similar to those used for sources, as described in Section II-D, except that a short carrier lifetime (requirement 5) is of utmost importance for both CW and pulsed operation [89]. Breakdown field strength (requirement 3), however, usually does not play any role in receiver structures.

An advantage of photoconductors is that they do not generate any noteworthy current in the absence of a THz signal and are therefore free of electrical shot noise. They are also highly resistive (requirement 4), even under illumination (resistance R_{ill}), resulting in a small thermal noise current $I_N = \sqrt{\frac{4k_B T}{R_{ill}}}$. Only laser noise may increase the overall system noise. CW photoconductive receivers have yet to reach a noise equivalent power of NEP = 1.8 fW/Hz at 188 GHz [93]. This leads to systems with very high dynamic ranges (DNRs). The highest CW DNR reported so far is 117 dB with 4 THz bandwidth or more at about 1hour and 11 minutes of measurement time [94].

TDS systems using 1550 nm lasers with ~90 fs pulses with classical, lumped-element devices yet reach DNRs beyond 110 dB with bandwidths beyond 6.5 THz [77], [78] with only 1–2 minutes of measurement time. By removing the InP host substrate, whose Reststrahlen-band starts absorbing around 6 THz, the authors of [95] have demonstrated a frequency coverage up to 10 THz.

In all cases, the required laser power to drive the lumped-element, antenna-coupled photoconductive receiver is in the range of 10–40 mW, yet it is achievable without amplifiers.

IV. ELECTRONIC TERAHERTZ SOURCES

The electronic implementation of THz sources is promising in terms of compactness, robustness, weight, and system efficiency. Furthermore, electronics can be easily mass-produced in scalable, cost-effective integrated circuit processes. The limit in electronic THz fundamental oscillator frequency is the speed of the active device, given by electron transit time and parasitic RC-time constants.

A. CMOS-BASED THZ SOURCES

Modern mobile THz systems, such as sensing and imaging systems, require chip-sized and cost-effective active THz components, i.e., intensely integrated circuits (ICs). Nanoscale CMOS and silicon germanium bipolar CMOS (SiGe BiCMOS) technologies offer high integration density, scalability, and compatibility with digital logic, making them preferable technologies for developing high-performance and low-cost electronic THz ICs.

The first demonstration of a CMOS THz source dates back to fifteen years ago, when a push-push oscillator was successfully developed to radiate an output power of about −42 dBm at 410 GHz using 45 nm CMOS technology [96]. Since that time, significant advancements in CMOS technology in terms of maximum frequency $f_{\max}$, DC-to-RF efficiency, and output power have been achieved.

THz CMOS sources can mainly be categorized into free-running oscillators, locked oscillators, or multiplier-chains.

CMOS THz sources that are based on a chain of phase-locked frequency multipliers with integrated antennas can generate signals up to 1.46 THz [97]. However, they suffer from poor DC-to-RF conversion efficiency, resulting in the need for high input power, which is challenging to obtain at frequencies beyond 100 GHz, and low output power. For example, the achieved output power of a multiplier chain implemented using 65 nm bulk CMOS was −15.1 dBm at 607.5 GHz [98] and −22.7 dBm at 1.33 THz [97]. For higher output power THz multiplier-chain-based sources, SiGe BiCMOS technology is used due to its advantages over CMOS, such as higher $f_T/f_{\max}$ and higher breakdown voltage. For example, an output power of −17 dBm at 823 GHz has been reached by using 250 nm BiCMOS with a SiGe HBT exhibiting a peak $f_t/f_{\max}$ of 280 GHz/435 GHz [99]. Furthermore, a similar output power of −17.3 dBm has been reported at a frequency of 928 GHz by implementing a 130 nm SiGe:C BiCMOS process with $f_t/f_{\max}$ values of 220/280 GHz [100].

In contrast to multiplier-chain-based CMOS sources, oscillator-based CMOS sources have a high DC-to-RF conversion efficiency, and thus, they can provide higher output power at frequencies below 300 GHz, whereas their output power quickly drops down to the μW level for higher frequencies if no power combining techniques are applied. For example, 65 nm CMOS THz sources with a single ring antenna providing an output power of about −2.74 dBm and −23 dBm at 293 GHz and 615.3 GHz, respectively, have been demonstrated [101], [102]. To enhance the radiated power of CMOS THz sources, coherent spatial power combining of an array of mutual coupling oscillators is employed [103], [104], [105], [106], [107]. Each oscillator resonates at the fundamental frequency and synchronizes correctly with the other oscillators. Therefore, the oscillators' harmonic signals radiate in phase and combine in space to create a focused beam. Using 65 nm bulk CMOS technology, a high-power arrayed source consisting of eight harmonic oscillators coupled via four 130 GHz quadrature oscillators has been shown to deliver 0.5 dBm at 260 GHz [108]. Moreover, even at frequencies beyond 300 GHz, coherent free-space power combining has helped to mitigate the rapid roll-off of single-antenna CMOS sources, as demonstrated in [103]. Here, an output power of −3 dBm at 694 GHz has been achieved from an array of 32 slot antennas that were realized in 45 nm CMOS technology. However, the majority of these scalable radiators are limited to frequencies below 600 GHz due to the fact that oscillator-based radiators above 600 GHz require a high ratio of fundamental oscillation frequency to maximum oscillation frequency (f_{osc}/f_{max}) and high-order harmonic power extraction and radiation.

For high-power THz sources beyond 600 GHz, high-speed 130 nm SiGe BiCMOS technology ($f_{\max}$ = 500 GHz) is employed. In [109], a synchronized two-dimensional (2D) oscillator array that consists of 42 coherent radiators has been realized. In this work, an output power of −10.7 dBm at 1.01 THz has been reached.

B. HETEROJUNCTION BIPOLAR AND HIGH ELECTRON MOBILITY TRANSISTORS

Aggressive device scaling has resulted thus far in gain cutoff frequencies around 700 GHz in silicon germanium heterojunction bipolar transistors (SiGe HBT) with ∼70 nm emitter width [110] and beyond 1 THz in InP HBT devices [111] with ∼130 nm emitter width. Compared to CMOS, both those bipolar technologies possess significant scaling potential compared to their technological size limits of around 10 nm. The high gain cutoff frequencies are attained in heterojunction bipolar transistors by several factors. The reduction of the total base resistance R_B, which consists of access resistance in the extrinsic semiconductor material and contact resistance, through very high p-doping in the base material. This becomes feasible only in the presence of an emitter-base heterointerface, which acts as an effective energy barrier in the valence band, preventing the diffusion of holes from the highly p-doped base into the emitter, thus maintaining high emitter injection efficiency and therefore high current gain even with a highly doped base. The heterointerface is created between the low-bandgap SiGe base material and the Si emitter, or the InGaAs base and the InP emitter, respectively. The power gain cutoff frequency $f_{\max}$ is relevant for the circuit operation frequency. As a rule of thumb, amplifier circuits may be operated up to $\frac{f_{max}}{3}$ with useful gain per stage, and fundamental oscillators up to $\frac{f_{max}}{2}$. The unity power gain frequency $f_{\max}$ can

be approximated in the bipolar transistor as:

$$f_{max} \approx \sqrt{\frac{f_t}{8\pi R_B C_{BC}}}$$

with the current gain cutoff frequency f_t, which relates to the transit time τ_F through the base and collector. f_t limits the instantaneous bandwidth of the amplifier circuit. To lower f_t, the base must be very thin, and the collector should be designed fully depleted. The collector thickness can be chosen to trade off $f_{\max}$ versus f_t, which inversely impacts breakdown voltage.

$$\frac{1}{2\pi \mathrm{f_t}} \approx \tau_\mathrm{F} + (\mathrm{C_{BE}}+\mathrm{C_{BC}}) \cdot \frac{\mathrm{kT}}{\mathrm{qI_C}} + \mathrm{C_{BC}} \cdot (\mathrm{R_E}+\mathrm{R_C})$$

The significance of capacitance reduction by lateral device scaling is visible in the equations above: C_{BC} acts as a negative feedback capacitance, both the intrinsic BC junction capacitance and extrinsic capacitive structures must be reduced to a minimum, and series resistances R_E and R_C must be minimal. The diffusive capacitance of the forward-biased base-emitter junction needs to be offset by a large absolute collector current I_C, which results in high current densities above 1 MA/cm^2 in geometrically scaled THz transistors [112]. Technological limits for scaling are given by minimum emitter width (currently around 70–130 nm), minimum contact resistance (around 10^{-8} Ωcm^2), near the physical limit, requiring extremely clean interfaces, and the trade-off between base sheet conductivity (also related to maximum p-type concentration) and base transit time.

SiGe HBT sources based on higher-order harmonic extraction could be operated at up to 1 THz [109], with a radiated output power of -11 dBm in a massively arrayed configuration and a conversion efficiency $< 10^{-4}$. The BiCMOS process enables complex integration suitable for integrated FMCW radar front-ends at 480 GHz [113], which exhibited a P_{out} of -16.5 dBm and 45 GHz bandwidth.

At 420 GHz, a radiated power of 10.3 dBm could be obtained from a SiGe chip that included spatial modulation capability [114]. Electronic THz pulse generation can be achieved with high bandwidth through reverse recovery of pin diodes, which are part of current BiCMOS processes. Frequency combs could be demonstrated, delivering an EIRP between -10 dBm at 200 GHz and -60 dBm at 1100 GHz via an on-chip patch antenna with a directivity between 24.6 dBi and 32 dBi between 330 GHz and 780 GHz [115].

In the InP material system, the narrow band base may be made from GaAsSb material instead of lattice-matched InGaAs. The antimonide-containing ternary GaAsSb forms a non-blocking type II heterojunction with InP and avoids the need for a compositional grading in the collector, which improves breakdown. Incorporating an optimized base-emitter structure, $f_{\max} > 1.2$ THz could be demonstrated recently, with more than 5 $V_{BD,CEO}$ [116]. InP high electron mobility transistors (HEMTs) exhibit the highest $f_{\max}$ around 1.5 THz, enabled by high electron mobility in the two-dimensional electron gas formed in a vertically confined InAs channel. This resulted in a demonstration of a nine-stage integrated amplifier operating at 850 GHz [117] and a ten-stage amplifier operating at 1 THz [118].

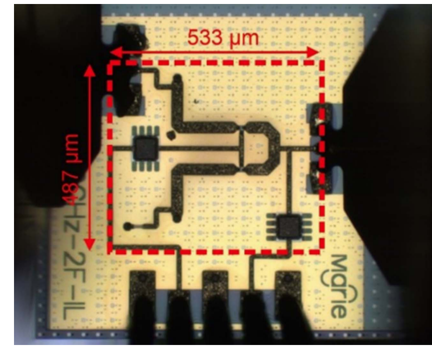

FIGURE 7. Chip photograph of InP HBT oscillator, left RF probe touching the port for subharmonic injection locking. From [124], © [2022] IEEE.

Metamorphic HEMT (mHEMT) devices with an InAs channel and a 20 nm gate length realized on a GaAs substrate exhibit $f_{\max} > 1.1$ THz [119]. InP-based HEMTs are known for their excellent noise performance, which has proven advantageous in mm-wave and sub-THz mixers and low-noise amplifiers for radio astronomy when operated at cryogenic temperatures [120]. An integrated mixer-amplifier InP HEMT source was demonstrated recently with 1.8 mW of output power at 680 GHz, exhibiting 0.1% DC-to-RF conversion efficiency [121]. In general, InP-based devices make use of high electron mobility and velocity in III/V compounds. The DC-to-RF conversion efficiency of transistor sources is strongly related to the ratio of device breakdown voltage to knee voltage drop. The high electron velocity in InP and related materials allows for relaxed device geometry, which, in conjunction with a high breakdown field, results in a large device breakdown voltage. This is especially true for the vertical HBT structure, which suffers less from surface breakdown compared to the HEMT. In the reported performance of sub-THz power amplifiers operating at 300 GHz for future 6G communications, an advantage of InP technologies, in particular InP HBT, is currently observable within a wider available data base [122]. InP HBT technology is equally promising for THz generation: fundamental InP HBT oscillators could be demonstrated up to 570 GHz, delivering close to 10 μW RF power [123]. InP HBT push-push oscillators can be tuned for efficient operation near the transistor's $f_{\max}$. Considering the system's use of oscillators, phase and frequency need to be controlled. An injection-locked InP HBT push-push oscillator shown in Fig. 7 could be demonstrated recently with 1.7% conversion efficiency and $>$ 0.5 mW output power at 420 GHz [124] with a transistor $f_{\max}$ of 450 GHz, enabling efficient THz sources with transistor scaling.

C. RESONANT TUNNELING DIODES

Beyond transistor technology, the resonant tunneling diode (RTD) represents a fundamental oscillator with an extremely

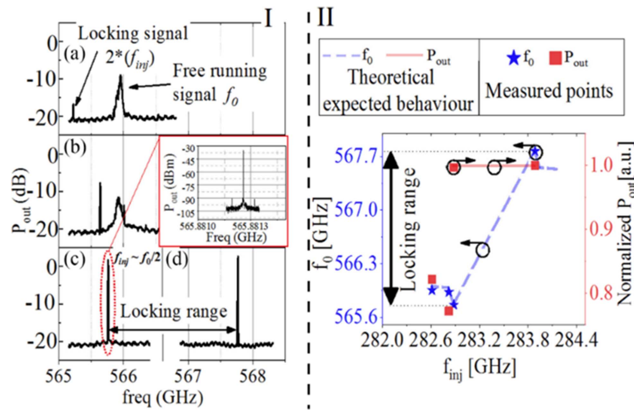

FIGURE 8. Spectrum of InP RTD oscillator subharmonic injection locking above 560 GHz. Within the locking range, the oscillator assumes the locking signal's linewidth (I). Under the locked condition, the peak spectral power increases about 14 dB (II). From [126], CC-BY-4.0, 2020.

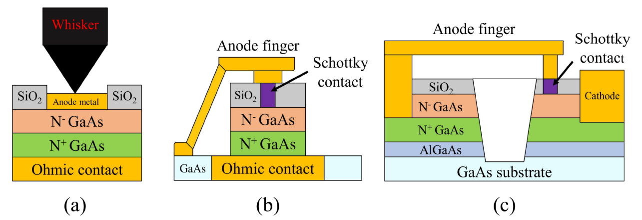

FIGURE 9. Types of Schottky contacts (a) Whisker contact, (b) Quasi-vertical planar contact, and (c) surface channel planar contact. Adapted from [128], CC-BY-4.0, 2022.

short transit time, owing to only a few nanometers separating the adjacent energy wells in the resonant tunnel diode structure. The RTD's IV-curve exhibits a region of negative differential conductance -*G*, formed by the superposition of the tunneling current through the barrier and the classical thermionic emission current across the barrier structure. -*G* represents an energy source in the surrounding LC oscillator tank. A chip-integrated narrowband antenna (patch or slot design) can be tuned to the RTD's complex impedance, resulting in very compact electronic THz sources. Thus far, InP RTD sources have been demonstrated with a fundamental oscillation frequency near 2 THz, representing the fastest solid-state oscillator available to date [125]. In many system applications, such as wireless communication links or spectroscopy, the oscillator frequency needs to be controlled precisely. For this purpose, subharmonic injection locking could be demonstrated in RTD devices operating beyond 0.5 THz, resulting in a narrow linewidth as shown in Fig. 8, and the ability to tune the oscillation frequency within the locking range [126].

Besides frequency and phase control of single sources, the injection locking process can be applied as mutual coupling between neighboring RTD or antenna pixels in order to realize dense phased arrays operating at THz frequencies. A recent demonstration of a 6 × 6 array radiated close to 12 mW at 450 GHz with 1% conversion efficiency [71]. The fixed phase relation between the pixels results in beamforming, and a directivity gain of near 24 dB could be observed. Further improvement to higher frequency and higher radiated power should be expected, considering the possibility of increasing the dissipated power in such an array at least tenfold before reaching thermal package limits and an at least four-fold increase in oscillation frequency.

D. SCHOTTKY-BARRIER DIODES

Since high-power amplifier technology is currently only capable of operating at frequencies close to 100 GHz, passive Schottky-barrier diode (SBD)-based frequency multipliers are a common method for obtaining powerful signals in the THz domain. SBDs are widely utilized as frequency multipliers to generate THz signals due to their attractive properties such as compactness, broadband operation, stable performance, and low power consumption [127], [128]. Typically, the epitaxial layer system of SBDs is grown either on GaAs or GaN substrates. Depending on the structure of the Schottky contact between the anode and metal, SBDs can be categorized into whisker-contacted and planar diodes, as demonstrated in Fig. 9 [128].

Whisker-contacted SBDs were employed as frequency multipliers to generate THz signals in the lower THz frequency band [129], [130]. However, the fragility of the whisker contacts made their assembly and integration complicated and thus prevented their widespread use. On the other hand, planar SBDs feature a planar Schottky contact structure that overcomes the drawback of the whisker-contacted ones. Planar SBDs comprise quasi-vertical planar SBDs [131] and surface channel planar SBDs [132]. Quasi-vertical planar SBDs suffer from high parasitic capacitance, which has significantly limited their implementation for THz frequency generation [133]. Contrary to quasi-vertical planar SBDs, planar channel ones exhibit extremely low parasitic capacitance [134], making them suitable for generating THz frequencies up to 8.7 THz [135]. Here, the corresponding measured RF performance revealed a series resistance of 15.4 Ω, a junction capacitance of 1.46 fF, and a cut-off frequency of 7 THz.

Benefiting from the nonlinear properties of the SBDs, they have been used either as frequency doublers or triplers to generate THz signals. Generally, the design of frequency doublers is simpler than that of frequency triplers, and they evidently have better conversion efficiency since they generate fewer harmonics. A variety of SBD-based frequency multipliers for THz generation have been reported in the literature. For example, in [136], a 332 GHz frequency doubler was developed, where the GaAs-based SBDs were hybridly integrated with the quartz-based microstrip-line (MSL) antenna. The maximum conversion efficiency was found to be 4.7% at 332.8 GHz. In addition, THz frequency triplers for 220 GHz and 440 GHz were demonstrated in [137], with corresponding conversion efficiencies of 16% and 12%, respectively. The developed stepped-impedance MSL low-pass filters for biasing the diodes and coupling the fundamental signal from the WR6-input (110–170 GHz) to the output WR2-output

(330–500 GHz) paved the way to design and implement THz frequency triplers. Passive frequency multiplying technologies have advanced significantly in the last decade, with conversion efficiencies of THz doublers and triplers of up to 30% and 20%, respectively, and a frequency bandwidth of 15–18% [138].

With increasing the operating frequency, the circuit size becomes smaller, and the hybrid integration technology becomes very lossy. Therefore, huge efforts were made to grow the antenna and DC-biasing circuitry together with the SBDs on the same substrate, i.e., monolithically, for higher output power at higher operational frequencies. As an example, a high-efficiency frequency tripler for generating THz signals between 540 GHz and 640 GHz was reported [139]. A 12 μm-thick GaAs substrate was utilized, and the achieved efficiency was between 4.5% and 9% at room temperature. In [140], a THz signal in the frequency range (2.48–2.75 THz) was generated using a monolithically integrated GaAs-based SBDs frequency cascaded tripler.

SBD-based frequency doublers and triplers can be cascaded to generate THz signals up to 2.75 THz [141]. For example, a 1.5 THz source consisting of a chain of four cascaded frequency doublers with a fundamental frequency of 88–99 GHz was reported in [142]. The maximum achieved output power was 40 μW. Furthermore, a four-channel source operating at 1.9 THz was demonstrated in [143], where a fundamental signal generator of 30-40 GHz together with two frequency doublers and two frequency triplers were used. Also here, the reported output power was 40 μW.

Cascaded multipliers were also employed to generate THz in the WR3-band. In [144], a 270–320 GHz source with 40 mW output power and an over 25% conversion efficiency of the last stage tripler was reported. Also in [145], an active multiplier chain with an output power of 250 mW at 260 GHz was reported.

However, the power-handling capability of multiplier modules is still a severe limiting factor, basically because of the limited dissipation of thermal energy produced during operation under relatively high power conditions. The thermal issue was addressed by many groups worldwide. Some researchers used highly thermally conductive sub-mounts for SBDs, such as high-resistive Si or AlN [146], [147]. Other bonded PECVD diamond layers on backside of the diode, greatly improved the heat dissipation and hence power-handling capability of the multiplier [148], [149].

An original technology solution has recently been developed by employing SBDs with monolithically integrated PECVD diamond heat spreaders [150], [151]. This approach is suitable not only for the fabrication of discrete diodes but also for the realization of so-called THz-MICs. THz-MICs assume fully integrated circuits with Schottky diodes and other passive surrounding circuitry, like filters, matching networks, and mechanical carrying elements, like an area carrier substrate, a diamond heat spreader, and supporting beam leads in the waveguide cavity. Such structures are preferred for frequencies above 500 GHz, where the assembly of discrete diodes on circuitry submounts is not accurate enough to provide reproducible results. Fig. 10 shows a THz-MIC structure as assembled in a metallic split-block for a 600 GHz tripler. This tripler has demonstrated up to 6% conversion efficiency and up to 4 mW of output power at about 600 GHz [150].

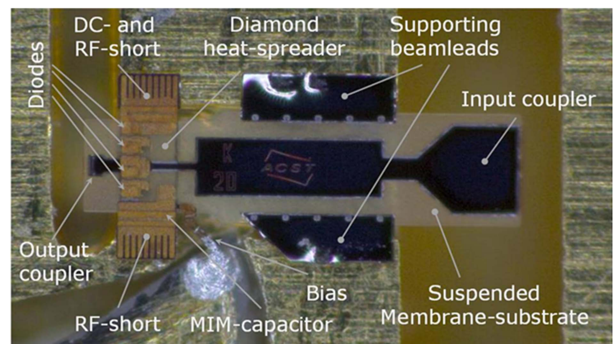

FIGURE 10. A 600 GHz tripler THz-MIC assembled in a metallic WG block. This approach provided conversion efficiency of up to 6% and output power up to 4 mW at around 600 GHz. From [150], CC BY-NC-ND, 2016.

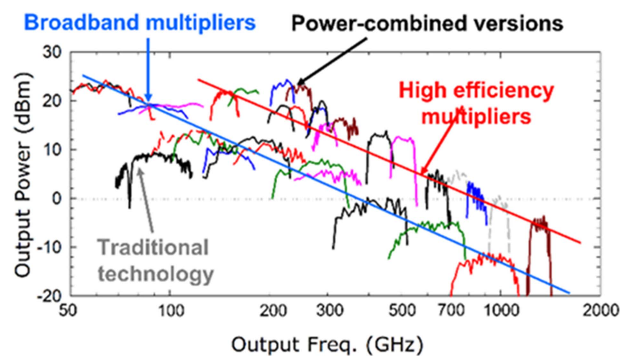

FIGURE 11. Comparative performance of high-power versus broadband THz sources based on passive frequency multipliers.

It is commonly known that there is a trade-off between the bandwidth and conversion efficiency of passive frequency multipliers. High-efficiency multipliers are optimized to provide maximal output power, whereas broadband multipliers target covering full WR frequency bands. Therefore, each type of multiplier source is employed for different target applications. Namely, broadband sources are used for measurement equipment or general applications, whereas high-power sources are used for applications where output power is of essential importance to reach the application goal, for instance, dynamic range. However, using the on-chip power combiner technique, broadband multipliers with up to ten times improved output power have been demonstrated [152]. Here, the achieved frequency range was between 0.16 THz and 1.6 THz, with a corresponding output power between 50 mW and 0.7 mW.

Fig. 11 comparatively summarizes a range of high-power sources versus broadband sources at frequencies up to 2 THz [138]. High-power and broadband sources are highlighted by red and blue lines, respectively. The interesting fact is that

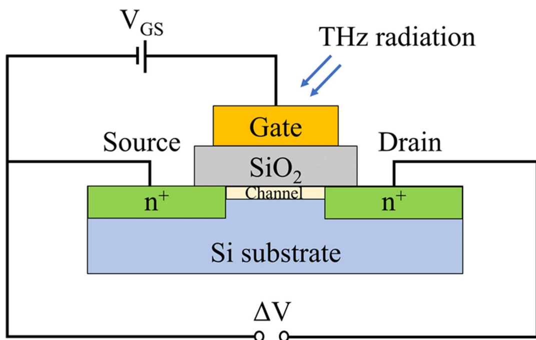

FIGURE 12. FET THz detector. Reprinted from [156], CC-BY-4.0, 2022.

both lines are nearly parallel in the logarithmic plot. Obviously, from this picture, full-band sources provide about 10 dB less output power in comparison to high-power options while performing within the full WR frequency bandwidth of about 40–45%. In contrast, high-power sources are built from high-efficiency but narrow-band passive multipliers. This approach allows for high output power but with a limited frequency bandwidth of nearly 10–20%. A noticeable increase in output power is possible by the so-called "in-phase power combining" approach [153], [154]. In-phase power combining can be implemented either on chip level, module level, or externally by coupling several multiplier modules by power splitters or combiners. All these results are achieved due to novel technology with an integrated diamond substrate or heat spreader and compare well to results achieved by traditional technology, assuming traditional planar Schottky diode arrays on a thin GaAs substrate.

V. ELECTRONIC TERAHERTZ RECEIVER

A. SCHOTTKY BARRIER DIODE DETECTORS

Schottky barrier diodes have been developed and optimized to be employed in THz systems not only as THz sources but also as THz direct detectors. The working principle of SBDs detectors is based on creating a depleted region at the semiconductor side of the semiconductor-metal junction, resulting in ultra-high sensitivity to the generated electron-hole pairs when the THz radiation interacts with the junction [155]. The volume of the depleted region can be determined by the applied reverse bias and the doping level of the semiconductor.

At room temperature, SBDs can provide a high responsivity of ($\sim$1 $\frac{\text{kV}}{\text{W}}$) and a low NEP of (1–50 $\frac{\text{pW}}{\text{Hz}^{1/2}}$) with a response time of about 20 ps [156]. Therefore, they have been intensively utilized as direct detectors for the THz radiation from 0.1 THz up to 10 THz [156]. Moreover, SBD arrays have been employed in THz imaging systems for real-time scanning receivers to improve the image quality [157], [158].

B. FIELD EFFECT TRANSISTORS

Dyakonov and Shur [159], [160] proposed the use of field effect transistors (FETs) to detect THz radiation in the early 1990s. Fig. 12 illustrates how a FET's channel between the source and drain can act as a resonator for plasma waves, where the dimensions of the channel determine the resonant frequency. For resonant frequency in the THz domain, the gate length has to be a few nanometers [156], [161]. The detection concept depends on the rectification of the induced alternating current (AC) by incoming THz radiation due to the nonlinear characteristics of the transistor. Consequently, a photoresponse proportional to the radiation power arises between the source and drain as a DC voltage (photovoltaic effect). Here, a source-drain asymmetry is required to induce the DC voltage for many reasons. For brevity, we direct the interested reader to the references [162], [163].

Over the last decade, the use of FETs to detect THz has significantly increased due to their enhanced performance. Generally, FET detectors have a NEP of about (10–100 $\frac{\text{pW}}{\text{Hz}^{1/2}}$), which is slightly higher than that of SBDs but better than that of thermal detectors at room temperature [156]. Furthermore, they can cover an ultra-wide frequency range from 0.1 THz up to 8 THz, and they are considered fast detectors with a response time of about 20 ps [156]. However, their responsivity is relatively small (0.1–0.4 $\frac{\text{kV}}{\text{W}}$) compared to SBDs. Recently, 2D materials like graphene and black phosphorus have been employed to develop far-infrared (FIR) detectors at room temperature up to 3 THz and low NEP THz cameras [164], [165]. However, with respect to NEP, the performance of graphene FET detectors is still inferior compared to CMOS FETs [156]. The last reported NEP of a room-temperature 32$\times$32 CMOS FET THz detector was about 12–14 $\frac{\text{pW}}{\text{Hz}}$ at a frequency range between 0.65 THz and 1 THz in 65 nm CMOS [165], i.e., 30 times lower than the best NEP (400 $\frac{\text{pW}}{\text{Hz}}$) that was achieved a decade ago [166].

C. HETERODYNE RECEIVERS

The motivation for developing heterodyne THz receivers can be traced back to the 1950s to enable the development of high-resolution terahertz spectroscopy systems needed for astronomical and atmospheric applications [167]. The operating principle of heterodyne receivers is based on mixing the incoming THz signal with another signal generated by a local oscillator (LO) to produce an intermediate frequency (IF) signal at the receiver's output [167], [168]. Typically, the IF signal is between DC and tens of GHz, allowing high-performance microwave components, such as amplifiers and filters, to process the detected signal. The main advantage of heterodyne receivers is that they maintain both the amplitude and phase information of the received THz signal [169], and thus, no complex techniques are required to retrieve the phase information. Furthermore, they feature low noise equivalent power (NEP) compared to thermal THz detectors such as bolometers and Golay cells, allowing them to detect even weak THz signals [169].

Usually, the nonlinear properties of semiconductor devices like SBDs, SIS junctions, hot electron bolometers (HEBs), and field effect transistors (FETs) are exploited to heterodyne the received THz signals with the LO signals [5], [170]. Here, the LO source has to provide sufficient LO power to drive the

mixer. Heterodyne THz receivers can be employed in either a coherent or incoherent configuration [171]. In the coherent approach, a common source is used to generate the RF and LO signals, and thus, coherent receivers provide higher sensitivity than incoherent ones. Here, the phase noise and frequency stability of the LO are crucial parameters because they impact the sensitivity and accuracy of the measurement system [167].

Several electronic-based solid-state sources have been used to generate the LO signal required for pumping heterodyne mixers. However, electronic-based sources like Gunn diodes suffer from low output power in the THz domain [172], whereas impact ionization avalanche transit-time (IMPATT) diodes [173] and frequency multipliers [174] suffer from high noise figure and high phase noise, respectively. In frequency multipliers, the signal from a low-frequency reference oscillator is multiplied [175], and thus the original phase noise of the low-frequency reference oscillator is increased by +6 dB for each frequency doubling [174]. On the other hand, photonic-based sources can provide the required LO signal either directly, such as gas lasers [176], [177] and QCLs [178], [179], [180], or by optical heterodyning using photoconductors and photodiodes [181], [182], [183].

In the past, gas lasers were widely employed as a LO source to pump heterodyne THz receivers due to their high output power (up to several hundreds of milliwatts) and ultra-broad operational frequency range (0.15–8 THz) [5]. However, the tuning complexity and bulky physical size of gas lasers have significantly constrained their integration with diode mixers for compact heterodyne THz receivers [167]. Also, optically pumped SBD and HEB mixers by QCL LO sources at frequencies higher than 2.5 THz have been demonstrated [178], [179], [180]. In contrast to gas lasers, QCLs are compact in size and simple to tune, and thus, they can be monolithically integrated with SBDs-mixers [178]. Moreover, QCLs can cover a wide THz range with tuning steps of a few GHz and sufficient output power up to 130 mW in CW operation. Even though many studies have been carried out to overcome the drawbacks of QCLs, such as the beam pattern quality [184], [185], [186] and single-mode operation [187], the required cooling system remains a major drawback for miniaturization, at least so far [167]. Despite that, QCL-based LOs have been employed successfully in airborne THz heterodyne receivers [50], [51], [52].

As an alternative to gas lasers and QCLs, optical heterodyne techniques can now be used to generate the LO signal for pumping THz heterodyne receivers. Recently, UTC-PDs were successfully employed to pump subharmonic THz SBD-mixers at room temperature [183], [188], [189]. It should be noted that even though the DSB noise temperature of SBD-mixers is higher compared to SIS and HEB mixers, they were preferred in the above-mentioned works since they do not require a cryogenic environment [167]. In earlier works reporting on optically pumped SBDs-mixers using UTC-PDs as LOs [183], [188], the achieved conversion loss (CL) was substantially higher than for electrically pumped subharmonic SBDs-mixers [190], [191], [192], [193], [194], [195], [196].

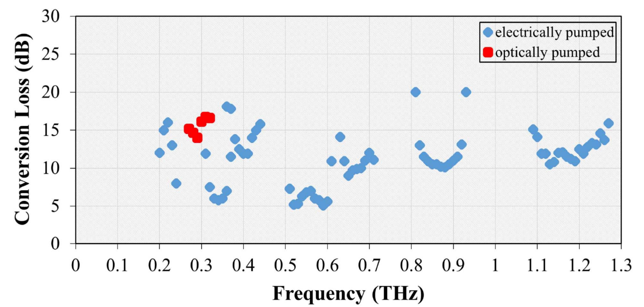

FIGURE 13. Conversion loss vs. RF for electrically pumped and optically pumped subharmonic THz SBD-mixers. Data from [189], [190], [191], [192], [193], [194], [195], [196].

This was mainly due to the low saturation output power of the UTC-PDs used. Recently, the use of high-performance MUTC-PDs reaching several mW output power has resulted in significantly lower CL levels, which are similar to those for electronically pumped mixers [189]. For comparison, Fig. 13 shows the experimentally achieved CL of electrically and optically pumped subharmonic THz SBD-mixers in the frequency range between 0.1 THz and 1.27 THz. In general, the approach of using optically pumped THz mixers enables accurate frequency tuning over an ultra-wide frequency range, room temperature operation, and the potential for monolithic integration. Depending on the laser source used, optically pumped heterodyne mixers may also benefit from the ultralow phase noise of optically generated LO signals. Recently, a record low phase noise below −170 dBc/Hz for a LO frequency of 12 GHz has been achieved by using mode-locked lasers [197]. Despite the complex technique required for stabilizing the free spectral range of the lasers and the carrier offset frequency, which cannot yet be integrated into chips, this achievement demonstrates the overall potential of the approach.

VII. CONCLUSION

This review article has shown that although terahertz technology is not brand new, significant achievements have only recently been revealed in this scientific field as a result of developments in semiconductor photonics and electronics. The first studies addressing the THz gap date back to the end of the 19th century, and numerous interactions between THz waves and matter have been studied. During the last century, mostly vacuum electron-based THz sources, including backward-wave oscillators, klystrons, gyrotrons, traveling-wave tubes, and free-electron lasers, were used for THz generation. With the advances in semiconductor technology, a variety of new high-performance semiconductor-based photonic and electronic THz sources and receivers are now available, with one major advancement: they are way smaller and easier to use. Examples reviewed in this article include photodiodes operated at room temperature, which now provide a mW output power level per single die at THz frequencies and cover a huge operational bandwidth in excess of 1 THz. Even higher THz

power levels are now available from cooled QCLs that were already successfully employed as LOs in heterodyne spectrometers. Difference frequency generation in mid-IR QCLs now even enables room-temperature operation.

On the electronic side, the oscillation frequencies of InP-based transistor technology have exceeded 1 THz. While InP HBTs may offer better DC-to-RF conversion efficiency due to their wide bandgap InP collector, HEMTs may be candidates for high-performance broadband THz LNAs. Also, the f_t and $f_{\max}$ of mainstream CMOS and SiGe HBT production processes allow the fabrication of THz sources and receivers.

Combining photonic and electronic semiconductor technologies opens the door to more functional THz devices. Examples include advanced THz low-barrier Schottky heterodyne mixers that can now be directly pumped using a single photodiode die or even THz mixers monolithically integrated with THz photodiodes. These breakthroughs may potentially pave the way towards new chip-size coherent THz front-ends.

THz waves are of interest because they are non-ionizing and non-invasive. Due to its low energy characteristics as compared to UV, THz radiation is harmless to humans and animals. Furthermore, it can penetrate many materials, so clothes are transparent to THz, which is exploited in security applications. Beyond that, the small wavelength compared to microwaves allow the fabrication of ultra-compact THz sources and receivers with tiny on-chip antennas. This allows the fabrication of arrays either by photonic integrated circuits (PICs) or RF ICs, for example, for enabling THz beam steering and other more functional THz circuits.

In general, the miniaturization of THz sources and receivers thanks to advances in semiconductor technology is not only beneficial for reducing their power consumption and cost but also for simplifying their use. Tiny THz sources and receivers would rather enable completely new innovative applications, for example, in medicine and agriculture. In-body THz imaging and spectroscopy or drones featuring THz sensors for observing plants can be envisaged. Also, more classical approaches, such as THz communications, benefit from the ever-increasing output power level and operational bandwidths, as well as the possibility of steering THz beams for future mobile communications. Radar sensors will soon reach distance resolutions way better than what is possible today, and THz imaging and spectroscopy systems will become way more compact and cheap.

In the future, we can expect the performance of semiconductor-based THz sources and receivers to further improve over time with respect to their key specifications, including output power, operational bandwidth, sensitivity, frequency stability, and phase noise. But beyond this, we may also see new functional devices such as monolithically integrated coherent THz transceivers or room-temperature-operated QCLs. PICs and RF ICs will enable the fabrication of THz beam steering transceivers. Heterogeneous integration, for example, between III-V gain materials, BiCMOS or SiGe electronics, and Si or SiN photonics, will enhance the device's functionality.

Moreover, reliable and low-loss innovative packaging solutions are developed. Especially the latter is key for moving THz technology from laboratories to daily life, to overcome existing challenges and reach the maturity and performance required for mass-market applications.

REFERENCES

[1] I. G. de Arrieta, "Beyond the infrared: A centenary of Heinrich Rubens's death," *Eur. Phys. J. H*, vol. 47, no. 1, 2022, Art. no. 11.
[2] H. Rubens and E. F. Nichols, "Heat rays of great wave length," *Phys. Rev. (Ser. I)*, vol. 4, no. 4, 1897, Art. no. 314.
[3] F. Sizov, "Brief history of THz and IR technologies," *Semicond. Phys., Quantum Electron. Optoelectron.*, vol. 22, no. 1, pp. 67–79, 2019.
[4] T. Nagatsuma, "Terahertz technologies: Present and future," *IEICE Electron. Exp.*, vol. 8, no. 14, pp. 1127–1142, 2011.
[5] H.-W. Hubers, "Terahertz heterodyne receivers," *IEEE J. Sel. Topics Quantum Electron.*, vol. 14, no. 2, pp. 378–391, Mar./Apr. 2008.
[6] U. U. Graf et al., "GREAT: The German first light heterodyne instrument for SOFIA," *Proc. SPIE*, vol. 6678, pp. 144–151, 2007.
[7] T. D. Graauw and F. Helmich, "Herschel-HIFI: The heterodyne instrument for the far-infrared," *Promise Herschel Space Observatory*, vol. 460, p. 45, 2001.
[8] E. H. T. Collaboration, "First M87 event horizon telescope results. I. The shadow of the supermassive black hole," 2019, *arXiv:1906.11238*.
[9] M. Tonouchi, "Cutting-edge terahertz technology," *Nature Photon.*, vol. 1, no. 2, pp. 97–105, 2007.
[10] M. V. Exter, C. Fattinger, and D. Grischkowsky, "Terahertz time-domain spectroscopy of water vapor," *Opt. Lett.*, vol. 14, no. 20, pp. 1128–1130, 1989.
[11] A. Roggenbuck et al., "Coherent broadband continuous-wave terahertz spectroscopy on solid-state samples," *New J. Phys.*, vol. 12, no. 4, 2010, Art. no. 043017.
[12] D. Bigourd et al., "Detection and quantification of multiple molecular species in mainstream cigarette smoke by continuous-wave terahertz spectroscopy," *Opt. Lett.*, vol. 31, no. 15, pp. 2356–2358, 2006.
[13] T. Nagatsuma, G. Ducournau, and C. C. Renaud, "Advances in terahertz communications accelerated by photonics," *Nature Photon.*, vol. 10, no. 6, pp. 371–379, 2016.
[14] E. S. Lee et al., "Semiconductor-based terahertz photonics for industrial applications," *J. Lightw. Technol.*, vol. 36, no. 2, pp. 274–283, Jan. 2018.
[15] E. Brown, K. McIntosh, K. Nichols, and C. Dennis, "Photomixing up to 3.8 thz in low-temperature-grown GaAs," *Appl. Phys. Lett.*, vol. 66, no. 3, pp. 285–287, 1995.
[16] R. Kohlhaas et al., "Photoconductive terahertz detectors with 105 dB peak dynamic range made of rhodium doped InGaAs," *Appl. Phys. Lett.*, vol. 114, no. 22, 2019, Art. no. 221103.
[17] C. Jördens, T. Schlauch, M. Li, M. Hofmann, M. Bieler, and M. Koch, "All-semiconductor laser driven terahertz time-domain spectrometer," *Appl. Phys. B*, vol. 93, pp. 515–520, 2008.
[18] K. Merghem, S. Busch, F. Lelarge, M. Koch, A. Ramdane, and J. Balzer, "Terahertz time-domain spectroscopy system driven by a monolithic semiconductor laser," *J. Infrared, Millimeter, Terahertz Waves*, vol. 38, pp. 958–962, 2017.
[19] K. Kolpatzeck et al., "System-theoretical modeling of terahertz time-domain spectroscopy with ultra-high repetition rate mode-locked lasers," *Opt. Exp.*, vol. 28, no. 11, pp. 16935–16950, 2020.
[20] T. Probst, A. Rehn, and M. Koch, "Compact and low-cost THz QTDS system," *Opt. Exp.*, vol. 23, no. 17, pp. 21972–21982, 2015.
[21] C. Brenner et al., "Compact diode-laser-based system for continuous-wave and quasi-time-domain terahertz spectroscopy," *Opt. Lett.*, vol. 35, no. 23, pp. 3859–3861, 2010.
[22] M. Scheller and M. Koch, "Terahertz quasi time domain spectroscopy," *Opt. Exp.*, vol. 17, no. 20, pp. 17723–17733, 2009.
[23] B. Sartorius, D. Stanze, T. Göbel, D. Schmidt, and M. Schell, "Continuous wave terahertz systems based on 1.5 μm telecom technologies," *J. Infrared, Millimeter, Terahertz Waves*, vol. 33, pp. 405–417, 2012.
[24] R. Wilk, F. Breitfeld, M. Mikulics, and M. Koch, "Continuous wave terahertz spectrometer as a noncontact thickness measuring device," *Appl. Opt.*, vol. 47, no. 16, pp. 3023–3026, 2008.

[25] S. Preu, G. Döhler, S. Malzer, L. Wang, and A. Gossard, "Tunable, continuous-wave terahertz photomixer sources and applications," *J. Appl. Phys.*, vol. 109, no. 6, 2011, Art. no. 061301.

[26] S. Hisatake, J.-Y. Kim, K. Ajito, and T. Nagatsuma, "Self-heterodyne spectrometer using uni-traveling-carrier photodiodes for terahertz-wave generators and optoelectronic mixers," *J. Lightw. Technol.*, vol. 32, no. 20, pp. 3683–3689, Oct. 2014.

[27] T. Kleine-Ostmann et al., "Continuous-wave THz imaging," *Electron. Lett.*, vol. 37, no. 24, 2001, Art. no. 1.

[28] S. Verghese, K. McIntosh, S. Calawa, W. Dinatale, E. Duerr, and K. Molvar, "Generation and detection of coherent terahertz waves using two photomixers," *Appl. Phys. Lett.*, vol. 73, no. 26, pp. 3824–3826, 1998.

[29] N. Kim et al., "Monolithic dual-mode distributed feedback semiconductor laser for tunable continuous-wave terahertz generation," *Opt. Exp.*, vol. 17, no. 16, pp. 13851–13859, 2009.

[30] C.-S. Friedrich et al., "New two-color laser concepts for THz generation," *IEEE J. Sel. Topics Quantum Electron.*, vol. 14, no. 2, pp. 270–276, Mar./Apr. 2008.

[31] Y. Hu, B. Khani, C. Brenner, V. Rymanov, A. Stöhr, and M. Hofmann, "Compact CW THz spectroscopy system and its application in water absorption measurements," in *Proc. IEEE Conf. Lasers Electro-Opt. Europe Eur. Quantum Electron. Conf.*, 2017, p. 1.

[32] J. O. Gwaro, C. Brenner, L. S. Theurer, M. Maiwald, B. Sumpf, and M. R. Hofmann, "Continuous wave THz system based on an electrically tunable monolithic dual wavelength Y-branch DBR diode laser," *J. Infrared, Millimeter, Terahertz Waves*, vol. 41, pp. 568–575, 2020.

[33] N. Surkamp et al., "Current tuned slotted Y-branch laser for wafer thickness measurements with THz radiation," *Electron. Lett.*, vol. 57, no. 24, pp. 936–938, 2021.

[34] B. B. Hu and M. C. Nuss, "Imaging with terahertz waves," *Opt. Lett.*, vol. 20, no. 16, pp. 1716–1718, 1995.

[35] P. U. Jepsen, D. G. Cooke, and M. Koch, "Terahertz spectroscopy and imaging–Modern techniques and applications," *Laser Photon. Rev.*, vol. 5, no. 1, pp. 124–166, 2011.

[36] M. Naftaly, N. Vieweg, and A. Deninger, "Industrial applications of terahertz sensing: State of play," *Sensors*, vol. 19, no. 19, 2019, Art. no. 4203.

[37] J. Balzer, T. Schlauch, A. Klehr, G. Erbert, G. Tränkle, and M. Hofmann, "High peak power pulses from dispersion optimised modelocked semiconductor laser," *Electron. Lett.*, vol. 49, no. 13, pp. 838–839, 2013.

[38] J. C. Balzer et al., "Passively mode-locked diode laser with optimized dispersion management," *IEEE J. Sel. Topics Quantum Electron.*, vol. 21, no. 6, pp. 16–23, Nov./Dec. 2015.

[39] C. Janke, M. Först, M. Nagel, H. Kurz, and A. Bartels, "Asynchronous optical sampling for high-speed characterization of integrated resonant terahertz sensors," *Opt. Lett.*, vol. 30, no. 11, pp. 1405–1407, 2005.

[40] R. Gebs, P. Klopp, G. Klatt, T. Dekorsy, U. Griebner, and A. Bartels, "Time-domain terahertz spectroscopy based on asynchronous optical sampling with femtosecond semiconductor disk laser," *Electron. Lett.*, vol. 46, no. 1, pp. 75–77, 2010.

[41] B. Döpke et al., "Asynchronous sampling terahertz time-domain spectroscopy using semiconductor lasers," *Electron. Lett.*, vol. 54, no. 10, pp. 640–641, 2018.

[42] T. Yasui, E. Saneyoshi, and T. Araki, "Asynchronous optical sampling terahertz time-domain spectroscopy for ultrahigh spectral resolution and rapid data acquisition," *Appl. Phys. Lett.*, vol. 87, no. 6, 2005, Art. no. 061101.

[43] C. Brenner et al., "Near infrared diode laser THz systems," *Adv. Radio Sci.*, vol. 16, pp. 167–175, 2018.

[44] J. Kutz, L. Liebermeister, N. Vieweg, K. Wenzel, R. Kohlhaas, and M. Naftaly, "A terahertz fast-sweep optoelectronic frequency-domain spectrometer: Calibration, performance tests, and comparison with TDS and FDS," *Appl. Sci.*, vol. 12, no. 16, 2022, Art. no. 8257.

[45] J. Faist, F. Capasso, D. L. Sivco, C. Sirtori, A. L. Hutchinson, and A. Y. Cho, "Quantum cascade laser," *Science*, vol. 264, no. 5158, pp. 553–556, 1994.

[46] H.-W. Hübers, H. Richter, M. Wienold, X. Lü, L. Schrottke, and H. T. Grahn, "Terahertz spectroscopy using quantum-cascade lasers," *Photoniques*, vol. 101, pp. 27–32, 2020.

[47] R. Köhler et al., "Terahertz semiconductor-heterostructure laser," *Nature*, vol. 417, no. 6885, pp. 156–159, 2002.

[48] B. Wen and D. Ban, "High-temperature terahertz quantum cascade lasers," *Prog. Quantum Electron.*, vol. 80, 2021, Art. no. 100363.

[49] A. Khalatpour, A. K. Paulsen, C. Deimert, Z. R. Wasilewski, and Q. Hu, "High-power portable terahertz laser systems," *Nature Photon.*, vol. 15, no. 1, pp. 16–20, 2021.

[50] H. Richter, M. Wienold, L. Schrottke, K. Biermann, H. T. Grahn, and H.-W. Hübers, "4.7-THz local oscillator for the GREAT heterodyne spectrometer on SOFIA," *IEEE Trans. Terahertz Sci. Technol.*, vol. 5, no. 4, pp. 539–545, Jul. 2015.

[51] C. Risacher et al., "The upGREAT dual frequency heterodyne arrays for SOFIA," *J. Astronomical Instrum.*, vol. 7, no. 4, 2018, Art. no. 1840014.

[52] M. Wienold et al., "The OSAS-B instrument: A balloon-borne heterodyne spectrometer for atomic oxygen in the mesosphere and lower thermosphere," in *Proc. 32nd IEEE Int. Symp. Space THz Technol.*, Baeza, Spain, 2022.

[53] H.-W. Hübers, R. Eichholz, S. Pavlov, and H. Richter, "High resolution terahertz spectroscopy with quantum cascade lasers," *J. Infrared, Millimeter, Terahertz Waves*, vol. 34, pp. 325–341, 2013.

[54] S. Jung et al., "Broadly tunable monolithic room-temperature terahertz quantum cascade laser sources," *Nature Commun.*, vol. 5, no. 1, 2014, Art. no. 4267.

[55] M. A. Belkin et al., "Room temperature terahertz quantum cascade laser source based on intracavity difference-frequency generation," *Appl. Phys. Lett.*, vol. 92, no. 20, 2008, Art. no. 201101.

[56] K. Fujita et al., "Recent progress in terahertz difference-frequency quantum cascade laser sources," *Nanophotonics*, vol. 7, no. 11, pp. 1795–1817, 2018.

[57] K. Fujita, S. Hayashi, A. Ito, T. Dougakiuchi, M. Hitaka, and A. Nakanishi, "Broadly tunable lens-coupled nonlinear quantum cascade lasers in the sub-THz to THz frequency range," *Photon. Res.*, vol. 10, no. 3, pp. 703–710, 2022.

[58] T. Ishibashi, N. Shimizu, S. Kodama, H. Ito, T. Nagatsuma, and H. Furata, "Uni-traveling-carrier photodiodes," *Japanese J. Appl. Phys.*, vol. 36, no. 10, pp. 6363–6368, 1997.

[59] T. Ishibashi and H. Ito, "Uni-traveling-carrier photodiodes," *J. Appl. Phys.*, vol. 127, no. 3, 2020, Art. no. 031101.

[60] T. Ishibashi and H. Ito, "Uni-traveling carrier photodiodes: Development and prospects," *IEEE J. Sel. Topics Quantum Electron.*, vol. 28, no. 2, Mar./Apr. 2022, Art. no. 3803006.

[61] C. C. Renaud, M. Natrella, C. Graham, J. Seddon, F. Van Dijk, and A. J. Seeds, "Antenna integrated THz uni-traveling carrier photodiodes," *IEEE J. Sel. Topics Quantum Electron.*, vol. 24, no. 2, Mar./Apr. 2018, Art. no. 8500111.

[62] A. Wakatsuki, Y. Muramoto, and T. Ishibashi, "Development of terahertz-wave photomixer module using a uni-traveling-carrier photodiode," *NTT Tech. Rev.*, vol. 10, no. 2, pp. 1–7, 2012.

[63] S. Makhlouf et al., "Monolithically integrated THz photodiodes with CPW-to-WR3 E-plane transitions for photodiodes packages with WR3-outputs," *J. Lightw. Technol.*, vol. 39, no. 24, pp. 7804–7812, Dec. 2021.

[64] T. Kurokawa, T. Ishibashi, M. Shimizu, K. Kato, and T. Nagatsuma, "Over 300 GHz bandwidth UTC-PD module with 600 GHz band rectangular-waveguide output," *Electron. Lett.*, vol. 54, no. 11, pp. 705–706, 2018.

[65] J. P. Seddon, M. Natrella, X. Lin, C. Graham, C. C. Renaud, and A. J. Seeds, "Photodiodes for terahertz applications," *IEEE J. Sel. Topics Quantum Electron.*, vol. 28, no. 2, Mar./Apr. 2022, Art. no. 3801612.

[66] M. Grzeslo et al., "High saturation photocurrent THz waveguide-type MUTC-photodiodes reaching mW output power within the WR3. 4 band," *Opt. Exp.*, vol. 31, no. 4, pp. 6484–6498, 2023.

[67] J.-M. Wun, H.-Y. Liu, Y.-L. Zeng, C.-L. Pan, C.-B. Huang, and J.-W. Shi, "High-power THz-wave generation by using ultra-fast (315 GHz) uni-traveling carrier photodiode with novel collector design and photonic femtosecond pulse generator," in *Proc. Opt. Fiber Commun. Conf.*, 2015, Paper M3C. 6.

[68] H. Ito et al., "High-power photonic millimetre wave generation at 100 GHz using matching-circuit-integrated uni-travelling-carrier photodiodes," *IEE Proc. Optoelectron.*, vol. 150, no. 2, pp. 138–142, 2003.

[69] P. Latzel et al., "Generation of mW level in the 300-ghz band using resonant-cavity-enhanced unitraveling carrier photodiodes," *IEEE Trans. Terahertz Sci. Technol.*, vol. 7, no. 6, pp. 800–807, Nov. 2017.

[70] R. A. Koala, M. Fujita, and T. Nagatsuma, "Nanophotonics-inspired all-silicon waveguide platforms for terahertz integrated systems," *Nanophotonics*, vol. 11, no. 9, pp. 1741–1759, 2022.

[71] Y. Koyama et al., "A high-power terahertz source over 10 mW at 0.45 THz using an active antenna array with integrated patch antennas and resonant-tunneling diodes," *IEEE Trans. Terahertz Sci. Technol.*, vol. 12, no. 5, pp. 510–519, Sep. 2022.

[72] M. Che, K. Kondo, H. Kanaya, and K. Kato, "Arrayed photomixers for THz beam-combining and beam-steering," *J. Lightw. Technol.*, vol. 40, no. 20, pp. 6657–6665, Oct. 2022.

[73] S. Makhlouf et al., "Novel 3-D multilayer terahertz packaging technology for integrating photodiodes arrays and rectangular waveguide-power combiners," *IEEE Trans. Microw. Theory Techn.*, vol. 68, no. 11, pp. 4611–4619, Nov. 2020.

[74] G. Carpintero, E. Garcia-Munoz, H. Hartnagel, S. Preu, and A. Raisanen, *Semiconductor Terahertz Technology: Devices and Systems at Room Temperature Operation*. Hoboken, NJ, USA: Wiley, 2015.

[75] E. Brown, "THz generation by photomixing in ultrafast photoconductors," *Int. J. High Speed Electron. Syst.*, vol. 13, no. 2, pp. 497–545, 2003.

[76] P.-K. Lu et al., "Ultrafast carrier dynamics in terahertz photoconductors and photomixers: Beyond short-carrier-lifetime semiconductors," *Nanophotonics*, vol. 11, no. 11, pp. 2661–2691, 2022.

[77] J. T. Darrow, X.-C. Zhang, D. H. Auston, and J. D. Morse, "Saturation properties of large-aperture photoconducting antennas," *IEEE J. Quantum Electron.*, vol. 28, no. 6, pp. 1607–1616, Jun. 1992.

[78] M. Beck et al., "Impulsive terahertz radiation with high electric fields from an amplifier-driven large-area photoconductive antenna," *Opt. Exp.*, vol. 18, no. 9, pp. 9251–9257, 2010.

[79] M. Martin and E. R. Brown, "Photoconductive materials for THz generation at 1550 nm: ErAs: GaAs vs InGaAs based materials," *Proc. SPIE*, vol. 9362, pp. 16–23, 2015.

[80] C. Baker, I. Gregory, M. Evans, W. Tribe, E. Linfield, and M. Missous, "All-optoelectronic terahertz system using low-temperature-grown InGaAs photomixers," *Opt. Exp.*, vol. 13, no. 23, pp. 9639–9644, 2005.

[81] B. Sartorius et al., "All-fiber terahertz time-domain spectrometer operating at 1.5 μm telecom wavelengths," *Opt. Exp.*, vol. 16, no. 13, pp. 9565–9570, 2008.

[82] R. Kohlhaas et al., "637 μ W emitted terahertz power from photoconductive antennas based on rhodium doped InGaAs," *Appl. Phys. Lett.*, vol. 117, no. 13, 2020, Art. no. 131105.

[83] U. Nandi, M. Scheer, H. Lu, J. C. Norman, A. C. Gossard, and S. Preu, "Bias-dependent carrier dynamics and terahertz performance of ErAs: In (Al) GaAs photoconductors," *IEEE Trans. Terahertz Sci. Technol.*, vol. 12, no. 4, pp. 353–362, Jul. 2022.

[84] C. W. Berry, N. Wang, M. R. Hashemi, M. Unlu, and M. Jarrahi, "Significant performance enhancement in photoconductive terahertz optoelectronics by incorporating plasmonic contact electrodes," *Nature Commun.*, vol. 4, no. 1, 2013, Art. no. 1622.

[85] V. Apostolopoulos and M. Barnes, "THz emitters based on the photodember effect," *J. Phys. D: Appl. Phys.*, vol. 47, no. 37, 2014, Art. no. 374002.

[86] P. Lu, D. Turan, and M. Jarrahi, "860 μW terahertz power generation from graded composition InGaAs photoconductive nanoantennas," in *Proc. IEEE/MTT-S Int. Microw. Symp.*, 2022, pp. 825–828.

[87] T. Seifert et al., "Efficient metallic spintronic emitters of ultrabroadband terahertz radiation," *Nature Photon.*, vol. 10, no. 7, pp. 483–488, 2016.

[88] U. Nandi et al., "Antenna-coupled spintronic terahertz emitters driven by a 1550 nm femtosecond laser oscillator," *Appl. Phys. Lett.*, vol. 115, no. 2, 2019, Art. no. 022405.

[89] E. Castro-Camus, L. Fu, J. Lloyd-Hughes, H. Tan, C. Jagadish, and M. Johnston, "Photoconductive response correction for detectors of terahertz radiation," *J. Appl. Phys.*, vol. 104, no. 5, 2008, Art. no. 053113.

[90] A. Ingar Romero, A. k. Mukherjee, A. Fernandez Olvera, M. Méndez Aller, and S. Preu, "Visualizing nanometric structures with sub-millimeter waves," *Nature Commun.*, vol. 12, no. 1, 2021, Art. no. 7091.

[91] B. L. Krause, A. D. J. F. Olvera, and S. Preu, "Photonic spectrum analyzer for wireless signals in the THz range," *IEEE Access*, vol. 10, pp. 42047–42054, 2022.

[92] A. d. J. F. Olvera et al., "Frequency selective optoelectronic downconversion of a terahertz pulse using ErAs: In (Al) GaAs photoconductors," *IEEE Access*, vol. 9, pp. 95391–95400, 2021.

[93] A. d. J. F. Olvera et al., "International system of units (SI) traceable noise-equivalent power and responsivity characterization of continuous wave ErAs: InGaAs photoconductive terahertz detectors," *Photonics*, vol. 6, no. 1, 2019, Art. no. 15.

[94] L. Liebermeister et al., "Optoelectronic frequency-modulated continuous-wave terahertz spectroscopy with 4 THz bandwidth," *Nature Commun.*, vol. 12, no. 1, 2021, Art. no. 1071.

[95] R. B. Kohlhaas et al., "Ultrabroadband terahertz time-domain spectroscopy using III-V photoconductive membranes on silicon," *Opt. Exp.*, vol. 30, no. 13, pp. 23896–23908, 2022.

[96] E. Seok et al., "A 410GHz CMOS push-push oscillator with an on-chip patch antenna," in *Proc. IEEE Int. Solid-State Circuits Conf. Tech. Papers*, 2008, pp. 472–629.

[97] Z. Ahmad, M. Lee, and K. O. Kenneth, "20.5 1.4 THz,− 13dBm-EIRP frequency multiplier chain using symmetric-and asymmetric-CV varactors in 65nm CMOS," in *Proc. IEEE Int. Solid-State Circuits Conf.*, 2016, pp. 350–351.

[98] B. Khamaisi, S. Jameson, and E. Socher, "A 0.58–0.61 THz single on-chip antenna transceiver based on active X30 LO chain on 65nm CMOS," in *Proc. IEEE 11th Eur. Microw. Integr. Circuits Conf.*, 2016, pp. 97–100.

[99] E. Öjefors, J. Grzyb, Y. Zhao, B. Heinemann, B. Tillack, and U. R. Pfeiffer, "A 820GHz SiGe chipset for terahertz active imaging applications," in *Proc. IEEE Int. Solid-State Circuits Conf.*, 2011, pp. 224–226.

[100] H. Aghasi, A. Cathelin, and E. Afshari, "A 0.92-thz SiGe power radiator based on a nonlinear theory for harmonic generation," *IEEE J. Solid-State Circuits*, vol. 52, no. 2, pp. 406–422, Feb. 2017.

[101] S. Jameson and E. Socher, "High efficiency 293 GHz radiating source in 65 nm CMOS," *IEEE Microw. Wireless Compon. Lett.*, vol. 24, no. 7, pp. 463–465, Jul. 2014.

[102] B. Khamaisi, S. Jameson, and E. Socher, "0.61 THz radiating source with on-chip antenna on 65nm CMOS," in *Proc. IEEE 11th Eur. Microw. Integr. Circuits Conf.*, 2016, pp. 389–392.

[103] L. Gao and C. H. Chan, "A 0.68–0.72-thz 2-D scalable radiator array with–3-dBm radiated power and 27.3-dBm EIRP in 65-nm CMOS," *IEEE J. Solid-State Circuits*, vol. 57, no. 10, pp. 3114–3124, Oct. 2022.

[104] Y. Tousi and E. Afshari, "A high-power and scalable 2-D phased array for terahertz CMOS integrated systems," *IEEE J. Solid-State Circuits*, vol. 50, no. 2, pp. 597–609, Feb. 2015.

[105] H. Jalili and O. Momeni, "A 0.46-thz 25-element scalable and wideband radiator array with optimized lens integration in 65-nm CMOS," *IEEE J. Solid-State Circuits*, vol. 55, no. 9, pp. 2387–2400, Sep. 2020.

[106] Y. Zhao et al., "A 0.54-0.55 THz 2× 4 coherent source array with EIRP of 24.4 dBm in 65nm CMOS technology," in *Proc. IEEE MTT-S Int. Microw. Symp.*, 2015, pp. 1–3.

[107] G. Guimarães and P. Reynaert, "A 670-GHz 4× 2 oscillator–radiator array achieving 7.4-dBm EIRP in 40-nm CMOS," *IEEE J. Solid-State Circuits*, vol. 56, no. 11, pp. 3399–3411, Nov. 2021.

[108] R. Han and E. Afshari, "A CMOS high-power broadband 260-GHz radiator array for spectroscopy," *IEEE J. Solid-State Circuits*, vol. 48, no. 12, pp. 3090–3104, Dec. 2013.

[109] Z. Hu, M. Kaynak, and R. Han, "High-power radiation at 1 THz in silicon: A fully scalable array using a multi-functional radiating mesh structure," *IEEE J. Solid-State Circuits*, vol. 53, no. 5, pp. 1313–1327, May 2018.

[110] B. Heinemann et al., "SiGe HBT with fx/fmax of 505 GHz/720 GHz," in *Proc. IEEE Int. Electron Devices Meeting*, 2016, pp. 3.1.1–3.1.4.

[111] M. Urteaga, R. Pierson, P. Rowell, V. Jain, E. Lobisser, and M. J. W. Rodwell, "130nm InP DHBTs with ft>0.52 thz and f max>1.1 THz," in *Proc. IEEE 69th Device Res. Conf.*, 2011, pp. 281–282.

[112] M. J. Rodwell, M. Le, and B. Brar, "InP bipolar ICs: Scaling roadmaps, frequency limits, manufacturable technologies," *Proc. IEEE*, vol. 96, no. 2, pp. 271–286, Feb. 2008.

[113] J. Wittemeier, F. Vogelsang, D. Starke, H. Rücker, and N. Pohl, "A SiGe based 0.48 THz signal source with 45 GHz tuning range," in *Proc. IEEE 51st Eur. Microw. Conf.*, 2022, pp. 869–872.

[114] R. Jain, P. Hillger, E. Ashna, J. Grzyb, and U. R. Pfeiffer, "A 64-pixel 0.42-THz source SoC with spatial modulation diversity for computational imaging," *IEEE J. Solid-State Circuits*, vol. 55, no. 12, pp. 3281–3293, Dec. 2020.

[115] S. Razavian and A. Babakhani, "Silicon integrated THz comb radiator and receiver for broadband sensing and imaging applications," *IEEE Trans. Microw. Theory Techn.*, vol. 69, no. 11, pp. 4937–4950, Nov. 2021.

[116] A. M. Arabhavi et al., "InP/GaAsSb double heterojunction bipolar transistor emitter-fin technology with f MAX= 1.2 THz," *IEEE Trans. Electron Devices*, vol. 69, no. 4, pp. 2122–2129, Apr. 2022.

[117] W. Deal, K. Leong, A. Zamora, V. Radisic, and X. B. Mei, "Recent progress in scaling InP HEMT TMIC technology to 850 GHz," in *Proc. IEEE MTT-S Int. Microw. Symp.*, 2014 pp. 1–3.

[118] X. Mei et al., "First demonstration of amplification at 1 THz using 25-nm InP high electron mobility transistor process," *IEEE Electron Device Lett.*, vol. 36, no. 4, pp. 327–329, Apr. 2015.

[119] A. Leuther et al., "20 nm metamorphic HEMT technology for terahertz monolithic integrated circuits," in *Proc. IEEE 9th Eur. Microw. Integr. Circuit Conf.*, 2014, pp. 84–87.

[120] G. Chattopadhyay et al., "A 340 GHz cryogenic amplifier based spectrometer for space based atmospheric science applications," in *Proc. IEEE 42nd Int. Conf. Infrared , Millimeter , Terahertz Waves*, 2017, pp. 1–2.

[121] A. Zamora et al., "A high efficiency 670 GHz x36 InP HEMT multiplier chain," in *Proc. IEEE MTT-S Int. Microw. Symp.*, 2017, pp. 977–979.

[122] H. Wang et al., "Power amplifiers performance survey 2000-present," Georgia Tech Electronics and Micro-System Lab (GEMS), version-6 release, Aug. 2021.

[123] M. Seo et al., "InP HBT IC technology for terahertz frequencies: Fundamental oscillators up to 0.57 THz," *IEEE J. Solid-State Circuits*, vol. 46, no. 10, pp. 2203–2214, Oct. 2011.

[124] A. Possberg et al., "An injection-lockable InP-DHBT source operating at 421 GHz with− 2.4 dBm output power and 1.7% DC-to-RF efficiency," in *Proc. IEEE/MTT-S Int. Microw. Symp.*, 2022, pp. 336–339.

[125] T. Maekawa, H. Kanaya, S. Suzuki, and M. Asada, "Oscillation up to 1.92 THz in resonant tunneling diode by reduced conduction loss," *Appl. Phys. Exp.*, vol. 9, no. 2, 2016, Art. no. 024101.

[126] K. Arzi et al., "Subharmonic injection locking for phase and frequency control of RTD-based THz oscillator," *IEEE Trans. Terahertz Sci. Technol.*, vol. 10, no. 2, pp. 221–224, Mar. 2020.

[127] I. Mehdi, J. V. Siles, C. Lee, and E. Schlecht, "THz diode technology: Status, prospects, and applications," *Proc. IEEE*, vol. 105, no. 6, pp. 990–1007, Jun. 2017.

[128] W. Kou et al., "A review of Terahertz sources based on Planar Schottky Diodes," *Chin. J. Electron.*, vol. 31, no. 3, pp. 467–487, 2022.

[129] T. Takada and M. Ohmori, "Frequency triplers and quadruplers with GaAs Schottky-barrier diodes at 450 and 600 GHz," *IEEE Trans. Microw. Theory Techn.*, vol. MTT-27, no. 5, pp. 519–523, May 1979.

[130] J. W. Archer, "Millimeter wavelength frequency multipliers," *IEEE Trans. Microw. Theory Techn.*, vol. MTT-29, no. 6, pp. 552–557, Jun. 1981.

[131] W. L. Bishop, K. McKinney, R. J. Mattauch, T. W. Crowe, and G. Green, "A novel whiskerless Schottky diode for millimeter and submillimeter wave application," in *Proc. IEEE MTT-S Int. Microw. Symp.*, 1987, pp. 607–610.

[132] A. Maestrini, D. Pukala, F. Maiwald, E. Schlecht, G. Chattopadhyay, and I. Mehdi, "Cryogenic operation of GaAs based multiplier chains to 400 GHz," in *Proc. 8th Int. Conf. THz Electron.*, Sep. 2000, pp. 81–84.

[133] C.-I. Lin et al., "Anti-parallel planar Schottky diodes for subharmonically-pumped 220 GHz/mixer," in *Proc. 10th Int. Symp. Space Terahertz Technol.*, 1999, Art. no. 85.

[134] S. Martin et al., "Fabrication of 200 to 2700 GHz multiplier devices using GaAs and metal membranes," in *Proc. IEEE MTT-S Int. Microw. Symp.*, 2001, pp. 1641–1644.

[135] L. Qian, A. Ning, and X. Tong, "Planar Schottky barrier diode with cut-off frequency of 8.7 THz," *J. Terahertz Sci. Electron. Inf. Technol.*, vol. 13, no. 5, pp. 679–683, 2015.

[136] H. Liu, J. Powell, C. Viegas, A. A. Cairns, and B. Alderman, "A 332GHz frequency doubler using flip-chip mounted planar schottky diodes," in *Proc. IEEE Asia-Pacific Microw. Conf.*, 2015, pp. 1–3.

[137] D. W. Porterfield, "High-efficiency terahertz frequency triplers," in *Proc. IEEE/MTT-S Int. Microw. Symp.*, 2007, pp. 337–340.

[138] Accessed: [Online]. Available: www.acst.de

[139] A. Maestrini et al., "A 540-640-GHz high-efficiency four-anode frequency tripler," *IEEE Trans. Microw. Theory Techn.*, vol. 53, no. 9, pp. 2835–2843, Sep. 2005.

[140] A. Maestrini et al., "Design and characterization of a room temperature all-solid-state electronic source tunable from 2.48 to 2.75 THz," *IEEE Trans. Terahertz Sci. Technol.*, vol. 2, no. 2, pp. 177–185, Mar. 2012.

[141] J. C. Pearson et al., "Demonstration of a room temperature 2.48–2.75 THz coherent spectroscopy source," *Rev. Sci. Instrum.*, vol. 82, no. 9, 2011, Art. no. 093105.

[142] G. Chattopadhyay et al., "An all-solid-state broad-band frequency multiplier chain at 1500 GHz," *IEEE Trans. Microw. Theory Techn.*, vol. 52, no. 5, pp. 1538–1547, May 2004.

[143] J. V. Siles et al., "A multi-pixel room-temperature local oscillator subsystem for array receivers at 1.9 THz," *Proc. SPIE*, vol. 9147, pp. 2275–2280, 2014.

[144] D. Moro-Melgar, O. Cojocari, and I. Oprea, "High power high efficiency 270–320 GHz source based on discrete Schottky diodes," in *Proc. IEEE 15th Eur. Radar Conf.*, 2018, pp. 337–340.

[145] E. Bryerton, S. Retzloff, and J. Hesler, "High-power submillimeter wave solid-state sources," in *Proc. IEEE 12th Glob. Symp. Millimeter Waves*, 2019, pp. 29–31.

[146] N. Alijabbari, M. F. Bauwens, and R. M. Weikle, "Design and characterization of integrated submillimeter-wave quasi-vertical Schottky diodes," *IEEE Trans. Terahertz Sci. Technol.*, vol. 5, no. 1, pp. 73–80, Jan. 2014.

[147] B. Alderman et al., "High power frequency multipliers to 330 GHz," in *Proc. IEEE 5th Eur. Microw. Integr. Circuits Conf.*, 2010, pp. 232–233.

[148] C. Lee et al., "Diamond heat-spreaders for submillimeter-wave GaAs Schottky diode frequency multipliers," in *Proc. 20th Int. Symp. Space Terahertz Technol.*, 2009, pp. 43–46.

[149] A. Y. Tang et al., "Steady-state and transient thermal analysis of high-power planar Schottky diodes," in *Proc. 22nd Int. Symp. Space Terahertz Technol.*, 2011, pp. 1–7.

[150] O. Cojocari, I. Oprea, H. Gibson, and A. Walber, "SubMM-wave multipliers by film-diode technology," in *Proc. IEEE 46th Eur. Microw. Conf.*, 2016, pp. 337–340.

[151] D. Moro-Melgar, O. Cojocari, I. Oprea, M. Hoefle, and M. Rickes, "Reliability and reproducibility of discrete Schottky diodes- based sources up to 370 ghz," in *Proc. IEEE 30th Int. Symp. Space THz Technol.*, 2019, p. 26.

[152] J. V. Siles, K. B. Cooper, C. Lee, R. H. Lin, G. Chattopadhyay, and I. Mehdi, "A new generation of room-temperature frequency-multiplied sources with up to 10× higher output power in the 160-GHz–1.6-THz range," *IEEE Trans. Terahertz Sci. Technol.*, vol. 8, no. 6, pp. 596–604, Jun. 2018.

[153] A. Maestrini et al., "In-phase power-combined frequency triplers at 300 GHz," *IEEE Microw. Wireless Compon. Lett.*, vol. 18, no. 3, pp. 218–220, Mar. 2008.

[154] J. V. Siles et al., "A single-waveguide in-phase power-combined frequency doubler at 190 GHz," *IEEE Microw. Wireless Compon. Lett.*, vol. 21, no. 6, pp. 332–334, Jun. 2011.

[155] I. Capan, "4H-SiC Schottky barrier diodes as radiation detectors: A review," *Electronics*, vol. 11, no. 4, 2022, Art. no. 532.

[156] A. Rogalski, "Progress in performance development of room temperature direct terahertz detectors," *J. Infrared, Millimeter, Terahertz Waves*, vol. 43, pp. 709–727, 2022.

[157] S.-P. Han et al., "Real-time continuous-wave terahertz line scanner based on a compact 1× 240 InGaAs Schottky barrier diode array detector," *Opt. Exp.*, vol. 22, no. 23, pp. 28977–28983, 2014.

[158] D. W. Park, E. S. Lee, J.-W. Park, H.-S. Kim, I.-M. Lee, and K. H. Park, "InGaAs Schottky barrier diode array detectors integrated with broadband antenna (Conference Presentation)," *Proc. SPIE*, vol. 10103, p. 53, 2017.

[159] M. Dyakonov and M. Shur, "Shallow water analogy for a ballistic field effect transistor: New mechanism of plasma wave generation by DC current," *Phys. Rev. Lett.*, vol. 71, no. 15, 1993, Art. no. 2465.

[160] M. Dyakonov and M. Shur, "Detection, mixing, and frequency multiplication of terahertz radiation by two-dimensional electronic fluid," *IEEE Trans. Electron Devices*, vol. 43, no. 3, pp. 380–387, Mar. 1996.

[161] L. J. Xu, F. C. Tong, X. Bai, and Q. Li, "Design of miniaturised on-chip slot antenna for THz detector in CMOS," *IET Microw., Antennas Propag.*, vol. 12, no. 8, pp. 1324–1331, 2018.

[162] W. Knap et al., "Terahertz emission by plasma waves in 60 nm gate high electron mobility transistors," *Appl. Phys. Lett.*, vol. 84, no. 13, pp. 2331–2333, 2004.

[163] W. Knap et al., “Field effect transistors for terahertz detection: Physics and first imaging applications,” *J. Infrared, Millimeter, Terahertz Waves*, vol. 30, pp. 1319–1337, 2009.
[164] H. Qin et al., “Room-temperature, low-impedance and high-sensitivity terahertz direct detector based on bilayer graphene field-effect transistor,” *Carbon*, vol. 116, pp. 760–765, 2017.
[165] U. R. Pfeiffer, J. Grzyb, H. Sherry, A. Cathelin, and A. Kaiser, “Toward low-NEP room-temperature THz MOSFET direct detectors in CMOS technology,” in *Proc. IEEE 38th Int. Conf. Infrared , Millimeter , Terahertz Waves*, 2013, pp. 1–2.
[166] U. R. Pfeiffer and E. Ojefors, “A 600-GHz CMOS focal-plane array for terahertz imaging applications,” in *Proc. IEEE 34th Eur. Solid-State Circuits Conf.*, 2008, pp. 110–113.
[167] Y.-J. Lin and M. Jarrahi, “Heterodyne terahertz detection through electronic and optoelectronic mixers,” *Rep. Prog. Phys.*, vol. 83, no. 6, 2020, Art. no. 066101.
[168] R. Lewis, “A review of terahertz detectors,” *J. Phys. D: Appl. Phys.*, vol. 52, no. 43, 2019, Art. no. 433001.
[169] A. Rogalski and F. Sizov, “Terahertz detectors and focal plane arrays,” *Opto-Electron. Rev.*, vol. 19, no. 3, pp. 346–404, 2011.
[170] R. Blundell and C. -y. E. Tong, “Submillimeter receivers for radio astronomy,” *Proc. IEEE*, vol. 80, no. 11, pp. 1702–1720, Nov. 1992.
[171] J. Li and J. Li, “Terahertz (THz) generator and detection,” *Elect. Sci. Eng.*, vol. 2, no. 1, pp. 11–25, 2020.
[172] A. Khalid et al., “A planar Gunn diode operating above 100 GHz,” *IEEE Electron Device Lett.*, vol. 28, no. 10, pp. 849–851, Oct. 2007.
[173] J. A. Nanzer, P. T. Callahan, M. L. Dennis, and T. R. Clark, “Photonic signal generation for millimeter-wave communications,” *Johns Hopkins APL Tech. Dig.*, vol. 30, no. 4, pp. 299–308, 2012.
[174] K. Saleh et al., “Phase noise performance comparison between optoelectronic oscillators based on optical delay lines and whispering gallery mode resonators,” *Opt. Exp.*, vol. 22, no. 26, pp. 32158–32173, 2014.
[175] A. Maestrini et al., “Schottky diode-based terahertz frequency multipliers and mixers,” *Comptes Rendus Physique*, vol. 11, no. 7/8, pp. 480–495, 2010.
[176] H.-W. Hübers et al., “Heterodyne receiver for 3-5 THz with hot-electron bolometer mixer,” *Z-Spec: A Broadband Millimeter-Wave Grating Spectrometer: Des., Construction, First Cryogenic Meas.*, vol. 5498, pp. 579–586, 2004.
[177] E. Gerecht et al., “Deployment of TREND: A low-noise receiver user instrument at 1.25 THz to 1.5 THz for AST/RO at the South Pole,” in *Proc. 14th Int. Symp. Space Terahertz Technol.*, 2003, pp. 179–188.
[178] M. C. Wanke et al., “Monolithically integrated solid-state terahertz transceivers,” *Nature Photon.*, vol. 4, no. 8, pp. 565–569, 2010.
[179] S. Shiba et al., “3.1-THz heterodyne receiver using an NbTiN hot-electron bolometer mixer and a quantum cascade laser,” *IEEE Trans. Terahertz Sci. Technol.*, vol. 2, no. 1, pp. 22–28, Jan. 2012.
[180] J. L. Kloosterman et al., “Hot electron bolometer heterodyne receiver with a 4.7-THz quantum cascade laser as a local oscillator,” *Appl. Phys. Lett.*, vol. 102, no. 1, 2013, Art. no. 011123.
[181] I. Cámara Mayorga et al., “Terahertz photonic mixers as local oscillators for hot electron bolometer and superconductor-insulator-superconductor astronomical receivers,” *J. Appl. Phys.*, vol. 100, no. 4, 2006, Art. no. 043116.
[182] I. C. Mayorga, A. Schmitz, T. Klein, C. Leinz, and R. Gusten, “First in-field application of a full photonic local oscillator to terahertz astronomy,” *IEEE Trans. Terahertz Sci. Technol.*, vol. 2, no. 4, pp. 393–399, Jul. 2012.
[183] P. G. Huggard et al., “1.55/spl mu/m photomixer sources for mm-wave heterodyne detection and frequency conversion with Schottky diodes,” in *Proc. IEEE LEOS Summer Topical Meetings*, 2005, pp. 105–106.
[184] M. I. Amanti, M. Fischer, G. Scalari, M. Beck, and J. Faist, “Low-divergence single-mode terahertz quantum cascade laser,” *Nature Photon.*, vol. 3, no. 10, pp. 586–590, 2009.
[185] G. Xu et al., “Efficient power extraction in surface-emitting semiconductor lasers using graded photonic heterostructures,” *Nature Commun.*, vol. 3, no. 1, 2012, Art. no. 952.
[186] A. W. M. Lee, Q. Qin, S. Kumar, B. S. Williams, Q. Hu, and J. L. Reno, “High-power and high-temperature THz quantum-cascade lasers based on lens-coupled metal-metal waveguides,” *Opt. Lett.*, vol. 32, no. 19, pp. 2840–2842, 2007.
[187] L. Xu, C. A. Curwen, P. W. Hon, Q.-S. Chen, T. Itoh, and B. S. Williams, “Metasurface external cavity laser,” *Appl. Phys. Lett.*, vol. 107, no. 22, 2015, Art. no. 221105.
[188] E. Rouvalis, M. J. Fice, C. C. Renaud, and A. J. Seeds, “Millimeter-wave optoelectronic mixers based on uni-traveling carrier photodiodes,” *IEEE Trans. Microw. Theory Techn.*, vol. 60, no. 3, pp. 686–691, Mar. 2012.
[189] S. Makhlouf, J. Martinez-Gil, M. Grzeslo, D. Moro-Melgar, O. Cojocari, and A. Stöhr, “High-power UTC-photodiodes for an optically pumped subharmonic terahertz receiver,” *Opt. Exp.*, vol. 30, no. 24, pp. 43798–43814, 2022.
[190] E. Ojefors, B. Heinemann, and U. R. Pfeiffer, “Subharmonic 220-and 320-ghz SiGe HBT receiver front-ends,” *IEEE Trans. Microw. Theory Techn.*, vol. 60, no. 5, pp. 1397–1404, May 2012.
[191] C. Wang et al., “Robust sub-harmonic mixer at 340 GHz using intrinsic resonances of hammer-head filter and improved diode model,” *J. Infrared, Millimeter, Terahertz Waves*, vol. 38, pp. 1397–1415, 2017.
[192] L. Ge et al., “0. 42 THz subharmonic mixer based on 3D precisely modeled diode,” *J. Infrared Millimeter Waves*, vol. 37, no. 3, pp. 338–343, 2018.
[193] B. Thomas et al., “An integrated 520–600 GHz sub-harmonic mixer and tripler combination based on GaAs MMIC membrane planar Schottky diodes,” in *Proc. IEEE 35th Int. Conf. Infrared, Millimeter , Terahertz Waves*, 2010, pp. 1–2.
[194] Y. He, Y. Tian, L. Miao, J. Jiang, and X. Deng, “A broadband 630–720 GHz Schottky based sub-harmonic mixer using intrinsic resonances of hammer-head filter,” *China Commun.*, vol. 16, no. 2, pp. 76–84, 2019.
[195] B. Thomas, A. Maestrini, D. Matheson, I. Mehdi, and P. De Maagt, “Design of an 874 GHz biasable sub-harmonic mixer based on MMIC membrane planar Schottky diodes,” in *Proc. IEEE 33rd Int. Conf. Infrared , Millimeter Terahertz Waves*, 2008, pp. 1–2.
[196] E. Schlecht et al., “Schottky diode based 1.2 THz receivers operating at room-temperature and below for planetary atmospheric sounding,” *IEEE Trans. Terahertz Sci. Technol.*, vol. 4, no. 6, pp. 661–669, Nov. 2014.
[197] X. Xie et al., “Photonic microwave signals with zeptosecond-level absolute timing noise,” *Nature Photon.*, vol. 11, no. 1, pp. 44–47, 2017.

SUMER MAKHLOUF received the master’s degree in communications engineering from the University of Duisburg-Essen, Duisburg, Germany, in 2018. He is currently working toward the Ph.D. degree in monolithically integrated THz photodiodes with rectangular waveguide outputs for coherent THz receivers. He is currently a Member of the Optoelectronics Department, Center for Semiconductor Technology and Optoelectronics (ZHO) and Research Associate with the University of Duisburg-Essen. Recently, he has been a Senior Engineer with Microwave Photonics GmbH, Oberhausen, Germany, working on developing RF modules for space communications and photonic integrated circuits for ultra-low phase noise THz systems.

OLEG COJOCARI received the Degree of Engineer in microelectronics and computer science from The Technical University of Moldova, Chisinau, Moldova, in 1995, and the Ph.D. degree in electrical engineering on the topic Schottky technology for terahertz electronics, in 2006. In 2000, he joined the Department of Microwave Engineering, Technical University of Darmstadt, Darmstadt, Germany. His research interests include the design, optimization, and fabrication of Schottky-based devices on III-V compound semiconductors for MM/SubMM wave applications, as well as development and optimization of the fabrication technology used therein. In 2006, he co-founded ACST GmbH, Hanau, Germany, which became the first European commercial supplier of Schottky diodes for THz-applications.

MARTIN HOFMANN received the Diploma in physics from Philipps-Universität Marburg, Marburg, Germany, in 1991, and the Ph.D. degree in gain dynamics of modelocked laser diodes with the group of Prof. Dr. Ernst Göbel, in 1994, and the Habilitation degree in experimental physics from the Philipps-Universität Marburg, in April 2000. In August 2001, he joined the Ruhr-Universität Bochum, Bochum, Germany, as a Professor of optoelectronic devices and materials. In 2008, he took over the chair for Photonics and Terahertz Technology also with Ruhr-Universität Bochum, Germany. From 1995 to spring 1996, he was a Postdoc at European Union Human Capital and Mobility Program, University College Cork, Cork, Ireland, Fondazione Ugo Bordoni, Rome, Italy, and Tele Danmark Research, Hoersholm, Denmark. From Spring 1996 to July 2001, he was a Research Assistant at the Group of Prof. Dr. Wolfgang Rühle, Max Planck Institute for Solid State Research in Stuttgart, Stuttgart, Germany, and with Philipps-Universität Marburg. He is the author or co-author of more than 400 publications in international journals or on international conferences on the fields of optoelectronic devices, THz technology, and modern optical systems.

TADAO NAGATSUMA (Fellow, IEEE) received the Ph.D. degree in electronic engineering from Kyushu University, Fukuoka, Japan, in 1986. From 1986 to 2007, he was at Nippon Telegraph and Telephone Corporation, Tokyo, Japan. Since 2007, he has been with Osaka University, Osaka, Japan, where he is currently a Professor with the Graduate School of Engineering Science. His research interests include millimeter-wave and terahertz photonics and their applications to wireless communications, sensing, and measurement. He is a Fellow of the Institute of Electronics, Information and Communication Engineers (IEICE), Tokyo. He is an Associate Editor for IEEE TRANSACTION ON TERAHERTZ SCIENCE AND TECHNOLOGY, President of the Terahertz Systems Consortium, and Past-Vice President of the IEICE.

SASCHA PREU (Member, IEEE) received the Diploma and Ph.D. degree (*summa cum laude*) in physics from the University of Erlangen-Nuremberg, Erlangen, Germany, in 2005 and 2009, respectively. From 2004 to 2010, he was at Max Planck Institute for the Science of Light, Erlangen. From 2010 to 2011, he was at the Materials and Physics Department, University of California at Santa Barbara, Santa Barbara, CA, USA, in the framework of a Feodor Lynen stipend by the Humboldt foundation. From 2011 to 2014, he was at the Chair of Applied Physics, University of Erlangen-Nuremberg. He is currently a Full Professor with the Department of Engineering and Information Technology, Technical University Darmstadt, Darmstadt, Germany, leading the Terahertz Devices and Systems Laboratory. His research interests include the development of semiconductor-based terahertz sources and detectors, including photomixers, photoconductors, and field-effect transistor rectifiers, development of powerful terahertz systems and applications of terahertz radiation.

NILS WEIMANN (Member, IEEE) received the Diploma (Hons.) in physics from the University of Stuttgart, Stuttgart, Germany, in 1996, and the Ph.D. degree in electrical engineering from Cornell University, Ithaca, NY, USA, in 1999. He was a Technical Manager at Alcatel Lucent's Bell Laboratories, Murray Hill, NJ, USA, till 2012, subsequently, he was leading the InP Devices Laboratory, Ferdinand-Braun-Institute, Berlin, Germany. In 2017, he was appointed Full Professor at the Faculty of Engineering, University of Duisburg-Essen, Duisburg, Germany, and chairing the Department of High Frequency Components. He is the author or co-author of more than 250 publications in international journals or on international conferences in the fields of RF devices and circuits, optoelectronic semiconductor technology, THz integration, and THz measurement techniques. He is currently chairing IEEE MTT TC-21, Terahertz Technology, and Applications Committee.

HEINZ-WILHELM HÜBERS received the Diplom degree and doctoral degree in physics from University Bonn, Germany, in 1991 and 1994, respectively. From 1991 to 1994, he was with the Max-Planck-Institute for Radioastronomy in Bonn, Germany. In 1994, he joined Deutsches Zentrum fr Luft- und Raumfahrt (German Aerospace Center, DLR) in Berlin, Germany, becoming head of department in 2001. From 2009 to 2014 he has been professor of experimental physics at Technical University Berlin, Germany, and head of the department "Experimental Planetary Physics" at DLR. In 2014, he became director of the Institute of Optical Sensor Systems at DLR and professor at Humboldt-University Berlin. His research interests are in THz physics and spectroscopy, particularly in THz systems for astronomy, planetary research, and security. Professor Hbers has authored or co-authored more than 200 refereed papers and the textbook "Terahertz Techniques". He has received the Innovation Award on Synchrotron Radiation (2003) and the Lilienthal Award (2007). In 2021, he received an honorary doctorate at Chalmers University of Technology, Gothenburg, Sweden.

ANDREAS STÖHR (Senior Member, IEEE) received the Dipl.-Ing. and Dr.-Ing. degrees in electrical engineering from Gerhard-Mercator University, Duisburg, Germany, in 1991 and 1997, respectively. From 1987 to 1996, he was the CEO of MS Steuerungsanlagen GmbH, Eppingen, Germany. From 1996 to 2013, he was a Research Scientist at the University of Duisburg-Essen (UDE), Duisburg. Between 1998 and 1999, he also joined the Communications Research Laboratory, Tokyo, Japan, where he worked on 60 GHz wireless systems employing radio over fiber techniques. He was also with France Telecom Orange Labs, France, in 2009, and Corning, in 2015. Since 2011, he has been a Professor and the Head of the Center for Semiconductor Technology and Optoelectronics (ZHO), Optoelectronics Department, UDE. He is currently a Visiting Professor with the University of Ottawa, Ottawa, ON, Canada. He has authored or coauthored more than 200 papers in refereed journals and conferences. His research interests include III/V integrated microwave photonic device technology and RF photonic integration technologies for millimeterwave and THz communications, measurement systems, and sensing applications. He is a Senior Member of the IEEE Photonics and MTT Society, a committee member and the chair of a number of international conferences, and the Guest Editor of IEEE/OSA.